Cellular/Molecular

TLR7 Negatively Regulates Dendrite Outgrowth through the Myd88 – c-Fos–IL-6 Pathway

Hsin-Yu Liu,[1,3] Yun-Fen Hong,[2,3] Chiao-Ming Huang,[3] Chiung-Ya Chen,[3] Tzyy-Nan Huang,[3] and Yi-Ping Hsueh[1,3]

[1]Graduate Institute of Life Sciences, National Defense Medical Center, Taipei 114, Taiwan, Republic of China, [2]Faculty of Life Sciences, Institute of Genome Sciences, National Yang-Ming University, Taipei 112, Taiwan, Republic of China, and [3]Institute of Molecular Biology, Academia Sinica, Taipei 115, Taiwan, Republic of China

Toll-like receptors (TLRs) recognize both pathogen- and danger-associated molecular patterns and induce innate immune responses. Some TLRs are expressed in neurons and regulate neurodevelopment and neurodegeneration. However, the downstream signaling pathways and effectors for TLRs in neurons are still controversial. In this report, we provide evidence that TLR7 negatively regulates dendrite growth through the canonical myeloid differentiation primary response gene 88 (Myd88)– c-Fos–interleukin (IL)-6 pathway. Although both TLR7 and TLR8 recognize single-stranded RNA (ssRNA), the results of quantitative reverse transcription-PCR suggested that TLR7 is the major TLR recognizing ssRNA in brains. In both *in vitro* cultures and *in utero* electroporation experiments, manipulation of TLR7 expression levels was sufficient to alter neuronal morphology, indicating the presence of intrinsic TLR7 ligands. Besides, the RNase A treatment that removed ssRNA in cultures promoted dendrite growth. We also found that the addition of ssRNA and synthetic TLR7 agonists CL075 and loxoribine, but not R837 (imiquimod), to cultured neurons specifically restricted dendrite growth via TLR7. These results all suggest that TLR7 negatively regulates neuronal differentiation. In cultured neurons, TLR7 activation induced IL-6 and TNF-α expression through Myd88. Using Myd88-, IL-6-, and TNF-α-deficient neurons, we then demonstrated the essential roles of Myd88 and IL-6, but not TNF-α, in the TLR7 pathway to restrict dendrite growth. In addition to neuronal morphology, TLR7 knockout also affects mouse behaviors, because young mutant mice ~2 weeks of age exhibited noticeably lower exploratory activity in an open field. In conclusion, our study suggests that TLR7 negatively regulates dendrite growth and influences cognition in mice.

Introduction

Toll-like receptors (TLRs), the most well studied pattern recognition molecules in innate immunity, are characterized by an extracellular leucine-rich repeat domain for ligand recognition and an intracellular toll/interleukin (IL)-1 receptor (TIR) domain for signaling (for review, see Takeda and Akira, 2004; Kawai and Akira, 2006; Huyton et al., 2007; Gauzzi et al., 2010; Kang and Lee, 2011). In mammals, 13 distinct TLRs have been classified. Among them, TLR3, TLR7, TLR8, and TLR9 have been shown to localize to intracellular endosomal vesicles (Nishiya and DeFranco, 2004; Jenkins and Mansell, 2010). These receptors recognize either engulfed DNA or RNA released from pathogens or neighboring dead cells. The intracellular materials in the endosome–lysosome pathways being recycled through autophagy also activate these receptors (Iwasaki, 2007; Lee et al., 2007; Czirr and Wyss-Coray, 2012). Specifically, TLR3 recognizes double-stranded RNA (Alexopoulou et al., 2001), while both TLR7 and TLR8 are activated by single-stranded RNA (ssRNA) (Diebold et al., 2004; Heil et al., 2004). TLR9 interacts with CpG oligodeoxynucleotides (Hemmi et al., 2000). All four of these TLRs play critical roles in innate immune responses (for review, see Bowie and Haga, 2005).

The TIR domains of TLRs interact with other TIR domain-containing adaptors, such as myeloid differentiation primary response gene 88 (Myd88), Myd88-adaptor-like, TIR domain containing adapter-inducing interferon (IFN)-β (TRIF), TRIF-related adaptor molecule, and sterile α and HEAT/Armadillo motif containing 1 (Sarm1), to regulate the downstream signaling pathways involved in the activation of transcription factors nuclear factor (NF)-κB, AP-1, and interferon regulatory factors. These transcription factors then control the expression of inflammatory and antiviral cytokines, including IL-6, IL-1β, tumor necrosis factor-α (TNF-α), and IFN-α/IFN-β (O'Neill and Bowie, 2007; Kumar et al., 2009).

In addition to innate immunity, TLRs have also been shown to regulate neurogenesis, neuronal morphogenesis, and neurodegeneration. For example, TLR2 is required for adult hippocampal neurogenesis, whereas TLR4 restricts neurogenesis and neuronal differentiation (Rolls et al., 2007). At the embryonic stage, TLR3 plays a negative role in the regulation of neuronal progenitor cell proliferation (Lathia et al., 2008). TLR3 activation also down-regulates neurite growth in cultured dorsal root ganglion ex-

Received Nov. 29, 2012; revised May 15, 2013; accepted June 5, 2013.

Author contributions: H.-Y.L., Y.-F.H., C.-Y.C., T.-N.H., and Y.-P.H. designed research; H.-Y.L., Y.-F.H., C.-M.H., and C.-Y.C. performed research; H.-Y.L., Y.-F.H., C.-M.H., and T.-N.H. analyzed data; H.-Y.L. and Y.-P.H. wrote the paper.

This work was supported by grants from Academia Sinica (to Y.-P.H.) and the National Science Council (NSC 99-2321-B-001-032, NSC 100-2321-B-001-022, NSC 101-2321-B-001-010, and NSC 98-2311-B-001-012-MY3 to Y.-P.H.). The authors declare no competing financial interests. We thank Drs. Ming-Zong Lai and Yung-Hsuan Wu, Mr. Ting-Fang Chou, and the Imaging Core of the Institute of Molecular Biology, Academia Sinica, for technical assistance; and Ms. Miranda Loney for English editing.

Correspondence should be addressed to Dr. Yi-Ping Hsueh, Institute of Molecular Biology, Academia Sinica, 128, Academia Road, Section 2, Taipei 115, Taiwan, Republic of China. E-mail: yph@gate.sinica.edu.tw.

DOI:10.1523/JNEUROSCI.5566-12.2013

 0270-6474/13/3311479-15$15.00/0

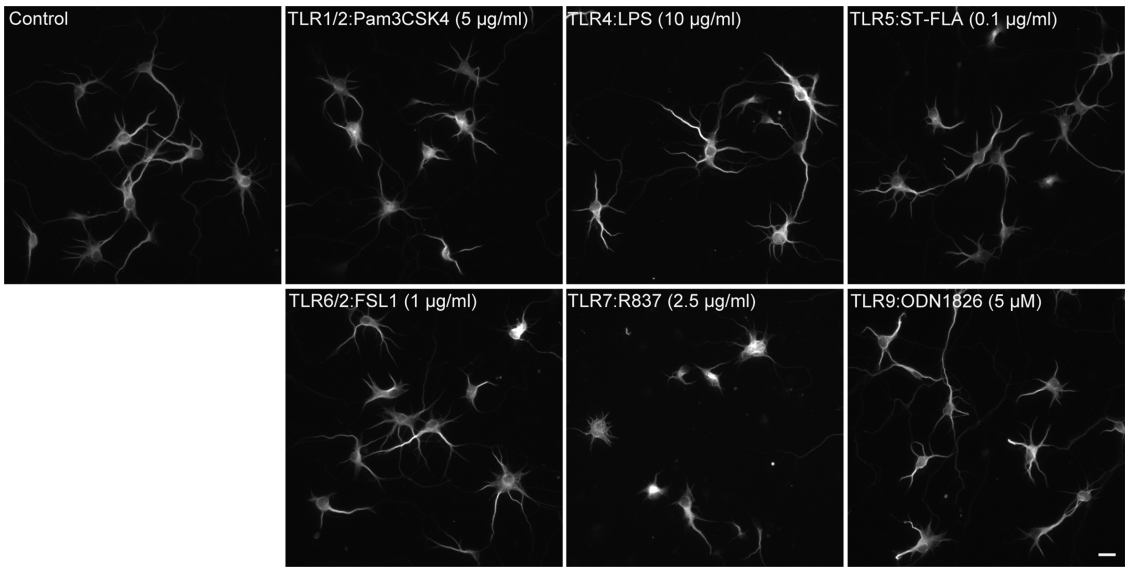

Figure 1. Effects of TLR agonists on dendritic morphology. The agonists of TLR1/2 (Pam3CysSerLys4, Pam3CSK4, a synthetic tripalmitoylated lipopeptide), TLR4 (LPS-EK, ultrapure LPS from *E. coli* K12), TLR5 (ST-FLA, Flagellin from *S. typhimurium*), TLR6/2 (FLS1, Pam2CGDPKHPKSF, a synthetic lipopeptide of *M. salivarium*), TLR7 (R837, i.e., imiquimod), and TLR9 (ODN1826, unmethylated CpG dinucleotides) were added to cultured mouse cortical neurons at 4 DIV. Cells were then fixed for immunostaining using a MAP2 antibody to monitor dendritic morphology at 6 DIV. Of these agonists, the TLR7 agonist R837 obviously impaired dendritic growth. Scale bar, 20 μm.

plants (Cameron et al., 2007). Additionally, TLR7 has recently been suggested to be involved in the regulation of neurodegeneration (Lehmann et al., 2012a,b).

Although it is clear that TLRs play roles in neural development and neurodegeneration, it is controversial whether the canonical TLR signaling pathways in innate immunity mediate the function of TLRs in neurons. For instance, the function of TLR3 and TLR8 in the downregulation of neurite outgrowth has been suggested to be independent of NF-κB and Myd88 (Ma et al., 2006; Cameron et al., 2007). However, Myd88 has been shown to be involved in TLR7-mediated neurodegeneration (Lehmann et al., 2012a,b). It is unclear whether these discrepancies are due to different TLRs or different cellular events.

In this report, we investigated whether and how TLR7 plays a role in neuronal morphogenesis. We found that TLR7 regulates neural development through the canonical Myd88–c-Fos–IL-6 pathway and controls cognition.

Materials and Methods

Animals. TLR7$^{-/-}$ (Lund et al., 2004), Myd88$^{-/-}$ (Hou et al., 2008), IL-6$^{-/-}$ (Kopf et al., 1994), TNF-$\alpha^{-/-}$ (Pasparakis et al., 1996), and TRIF mutant mice (Hoebe et al., 2003) in a C57BL/6 genetic background were imported from the Jackson Laboratory and were housed in the animal facility of the Institute of Molecular Biology, Academia Sinica, under pathogen-free conditions and a 14/10 h light/dark cycle with controlled temperature and humidity. All animal experiments were performed with the approval of the Academia Sinica Institutional Animal Care and Utilization Committee, and in strict accordance with its guidelines and those of the Council of Agriculture Guidebook for the Care and Use of Laboratory Animals. The sample size for each experiment was labeled in figures or described in corresponding figure legends.

Chemicals and antibodies. ssRNA-double right (DR), CL075, R837, loxoribine, Pam3CysSerLys4 (Pam3CSK4, a synthetic tripalmitoylated lipopeptide), LPS-EK (ultrapure LPS from *Escherichia coli* K12), ST-FLA (Flagellin from *Salmonella typhimurium*), FLS1 (Pam2CGDPKHPKSF, a synthetic lipopeptide of *Mycoplasma salivarium*), and ODN1826 (unmethylated CpG dinucleotides) were purchased from InvivoGen; bovine serum albumin (BSA) was purchased from Sigma-Aldrich; RNase A was purchased from Invitrogen and Qiagen. Tetrodotoxin (TTX) and NMDA were purchased from Tocris Bioscience. Recombinant mouse IL-6 was purchased from R&D Systems (12.5 U/ng; Gilmore et al., 2004). The following antibodies were used: rabbit polyclonal GFP (Invitrogen); rabbit polyclonal MAP2 (Millipore); mouse monoclonal MAP2 (Sigma-Aldrich); mouse monoclonal SMI-312R (Covance); rat monoclonal HA (Roche); mouse monoclonal valosin-containing protein (VCP; BD Biosciences); mouse β-tubulin (Sigma-Aldrich); rabbit polyclonal c-*fos* (9F6; Cell Signaling Technology); rat monoclonal IgG1 isotype control and rat monoclonal IL-6 neutralizing antibodies (R&D Systems); HRP-conjugated secondary antibodies (GE Healthcare); and Alexa Fluor 488- and Alexa Fluor 594-conjugated secondary antibodies (Invitrogen).

Plasmids. The full-length HA-tagged TLR7 construct pUNO1-TLR7-HAx3 was purchased from InvivoGen. The plasmid UNO1 was used as the vector control for pUNO1-TLR7-HAx3. To quantify the actual copy numbers of TLR7 and TLR8 transcripts, the fragments of TLR7 ($-74 \sim 326$) and TLR8 ($-31 \sim 293$) that cover the target sites of the primers for real-time PCR were subcloned into a pDrive cloning vector and used as the standard templates. For the miRNA constructs, the target sequences of TLR7 designed by the BLOCK-iT RNAi Designer tool (Invitrogen) were as follows: miR-TLR7-#1, 5′-CAG GTC TAC CAT GCA TCT ATA-3′; and miR-TLR7-#2, 5′-ACC ATG GAA AGT GAC TCT CTT-3′. The paired oligonucleotides were inserted into a pcDNA 6.2-GW/EmGFP-miR vector using the BLOCK-iT Pol II miR RNAi Expression Vector Kit (Invitrogen). A plasmid pcDNA 6.2-GW/EmGFP-miR-neg (miR-ctrl, Invitrogen) predicted to not target any vertebrate gene was used as a negative control. For the *in utero* electroporation (IUE), the miRNA fragment from pcDNA 6.2-GW/EmGFP-miR TLR7-#1 was subcloned into the 3′ untranslated region of the plasmid pCAG-GFP (Addgene plasmid 11150; Matsuda and Cepko, 2004). The plasmid CAG-GFP-miR-TLR7#1 was then used for *in utero* electroporation. To outline the neuronal morphology of cultured neurons, plasmid cDNA 6.2-GW/EmGFP-miR-neg, which expresses Emerald-GFP, was cotransfected with the indicated constructs into cultured neurons.

Cell culture and transfection. Cortical neurons from embryonic day 17.5 (E17.5) mouse embryos of either sex were cultured in Neurobasal medium/DMEM (1:1) with B27 supplement and transfected using the calcium phosphate precipitation method as described previously (Lin et al., 2007). Under these conditions, the cultures contained $0.92 \pm 0.11\%$ GFAP+ astrocytes and $0.39 \pm 0.04\%$ IbaI+ microglia examined at 4 d *in vitro* (DIV). To investigate the neuronal morphology resulting from wild-type (WT) and TLR7 knock-out (KO) or Myd88 KO, cultured neurons from littermates were compared to minimize the variations. Each

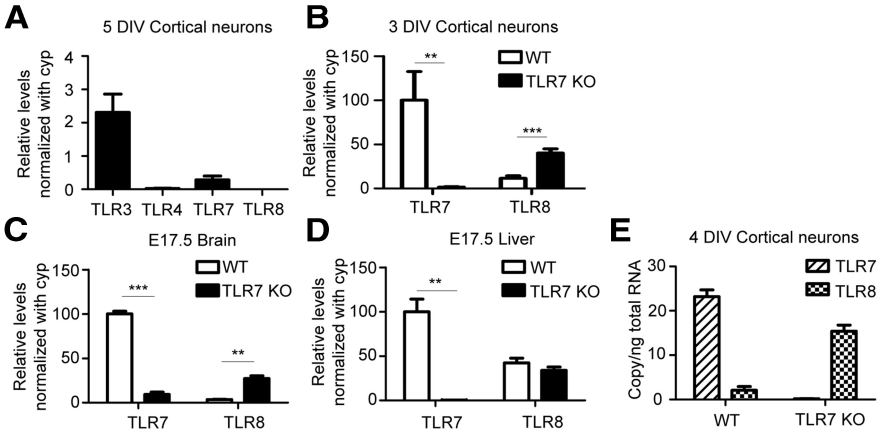

Figure 2. Differential expression of TLR7 and TLR8 in mouse neurons. ***A***, The expression of TLR3, TLR4, TLR7, and TLR8 in WT cortical neurons at 5 DIV. ***B–D***, The expression of TLR7 and TLR8 in WT and TLR7 KO cortical neurons (***B***), E17.5 brain (***C***), and E17.5 liver (***D***). The relative levels of TLRs were determined by quantitative RT-PCR using Cyp as an internal control. All of the values were normalized with WT TLR7 (as 100). ***E***, The actual copy numbers of TLR7 and TLR8 transcripts in cultured cortical neurons. The experiments were independently repeated at least three times. Error bars represent the mean + SD. $^{**}p < 0.01$; $^{***}p < 0.001$.

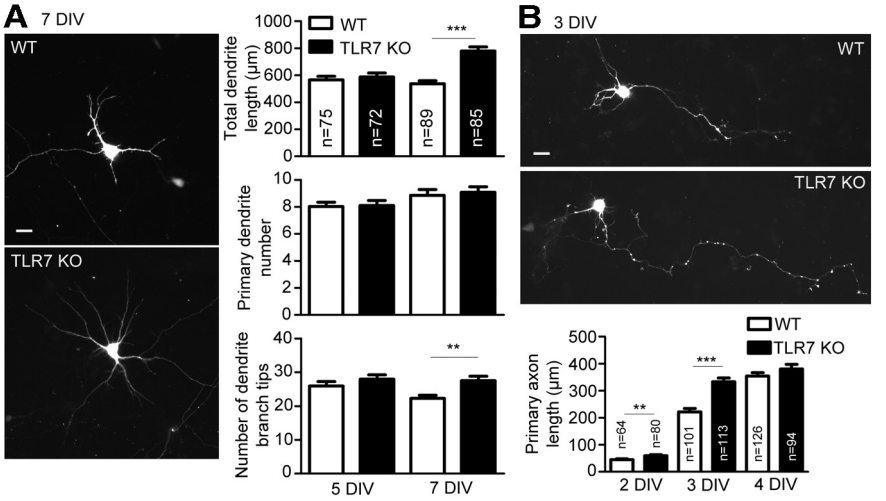

Figure 3. Deletion of TLR7 promotes dendrite and axon growth in cultured cortical neurons. ***A***, Compared with WT neurons, TLR7 KO neurons have longer dendrite lengths and more dendrite branch tips at 7 DIV, but not at 5 DIV. There was no difference between WT and TLR7 KO primary dendrite number. ***B***, The primary axon length of TLR7 KO neurons is longer than those of WT neurons before 4 DIV. Transfection with EGFP was performed at 4 DIV (***A***) and 1 DIV (***B***). Immunostaining with both EGFP and SMI-312R or MAP2 antibodies was performed to outline neuronal morphology and identify axons and dendrites, although only the EGFP signals are shown. Scale bar, 20 μm. The data represent the mean + SEM. The numbers of analyzed neurons are indicated in columns. $^{**}p < 0.01$; $^{***}p < 0.001$.

experiment was repeated at least three times. The cell density was controlled at 2.5–3 $\times$ 10^5 cells/well in 12-well plates with 18 mm poly-L-lysine-coated coverslips. Transfection with an EGFP expression construct was performed to outline the neuronal morphology. HEK293T cells were grown in DMEM supplemented with 10% FBS at 37°C and 5% CO_2. Transfection of HEK293T cells was performed using Lipofectamine (Invitrogen).

Relative and absolute quantitative RT-PCR. To prepare total RNA from cultured cortical neurons, neurons were plated at a density of 1 $\times$ 10^6 cells/well in poly-L-lysine-coated six-well plates. Cultured neurons and different mouse tissues at E17.5 were subjected to RNA extraction using Trizol reagent according to the manufacturer's instructions (Invitrogen) followed by DNase I (New England BioLabs) digestion for 30 min at 37°C to remove contaminating DNA. Three micrograms of total RNA from cultured cortical neurons and 5 μg from mouse tissues were then used for cDNA synthesis by the Transcriptor First Strand cDNA Synthesis Kit (Roche) with an oligo(dT)18 primer. A real-time PCR assay was performed using the LightCycler480 (Roche) and the Universal ProbeLibrary probes (UPL; Roche) system. The primers and their paired probes were designed using the Assay Design Center Web Service (http://qpcr.probefinder.com/roche3.html) and were as follows: TLR3-F, 5′-GAT ACA GGG ATT GCA CCC ATA-3′, and TLR3-R, 5′-TCC CCC AAA GGA GTA CAT TAG A-3′, with the UPL Probe #26; TLR4-F, 5′-GGA CTC TGA TCA TGG CAC TG-3′, and TLR4-R, 5′-CTG ATC CAT GCA TTG GTA GGT-3′, with the UPL Probe #2; TLR7-F, 5′-TGA TCC TGG CCT ATC TCT GAC-3′, and TLR7-R, 5′-CGT GTC CAC ATC GAA AAC AC-3′, with the UPL Probe #25; TLR8-F, 5′-CAA ACG TTT TAC CTT CCT TTG TCT-3′, and TLR8-R, 5′-ATG GAA GAT GGC ACT GGT TC-3′, with the UPL Probe #56; IL-6-F, 5′-GCT ACC AAA CTG GAT ATA ATC AGG A-3′, and IL-6-R, 5′-CCA GGT AGC TAT GGT ACT CCA GAA-3′, with the UPL Probe #6; TNF-F, 5′-TCT TCT CAT TCC TGC TTG TGG-3′, and TNF-R, 5′-GGT CTG GGC CAT AGA ACT GA-3′, with the UPL Probe #49; IL-1β-F, 5′-AGT TGA CGG ACC CCA AAA G-3′, and IL-1β-R, 5′-AGC TGG ATG CTC TCA TCA GG-3′, with the UPL Probe #38; IFNb1-F (pair 1), 5′-CTG GCT TCC ATC ATG AAC AA-3′, and IFNb1-R (pair 1), 5′-AGA GGG CTG TGG TGG AGA A-3′, with the UPL Probe #18; IFNb1-F (pair 2), 5′-CAC AGC CCT CTC CAT CAA CTA-3′, and IFNb1-R (pair 2), 5′-CAT TTC CGA ATG TTC GTC CT-3′, with the UPL Probe #78; and Cyclophilin-F, 5′-TGC CCA GCA GTT TAG TAC CC-3′, and Cyclophilin-R, 5′-TGC TTC CCT GTC TCC ACA GT-3′, with the UPL Probe #64. The PCR thermal profile was set as follows: denaturation at 95°C for 10 min; 45 cycles of denaturation at 95°C for 10 s, annealing at 60°C for 30 s, and extension at 72°C for 1 s; and a final cooling step at 40°C for 30 s. To obtain the actual copy numbers of the TLR7 and TLR8 transcripts, the pDrive-TLR7 (−74 ~ 326) and pDrive-TLR8 (−31 ~ 293) plasmids were serially diluted 10-fold as standards. The corresponding copy numbers were calculated using a previously described formula (Whelan et al., 2003).

ELISA. Supernatants were collected from cultured cortical neurons at 2.5 $\times$ 10^6 cells/well in poly-L-lysine-coated six-well plates. Each treatment was triplicated in three wells in a single experiment, and the experiments were repeated at least twice. The quantitative determination of cytokines was performed using mouse IL-6 and TNF-α ELISA Ready-SET-GO Kit (eBioscience) and mouse IL-1β ELISA Set (BD Biosciences) according to the manufacturer's instructions.

Immunofluorescence staining. Primary cultured neurons were fixed with 4% PFA and 4% sucrose in PBS for 15 min at room temperature. After washing with PBS, the cells were permeabilized with 0.1% Triton X-100 (Sigma-Aldrich) in PBS for 10 min at room temperature and were blocked with 5% BSA in PBS for 30 min. The fixed neurons were incubated with primary antibodies diluted in 5% BSA/PBS buffer overnight at 4°C. After washing with PBS containing 0.1% Tween 20, the neurons were incubated with Alexa Fluor 488- and Alexa Fluor 594-conjugated secondary antibodies for 1 h at room temperature. Samples were then mounted with Vectashield mounting medium (H-1000; Vector Laboratories) and visualized with an Axio Imager-Z1 microscope (Carl Zeiss)

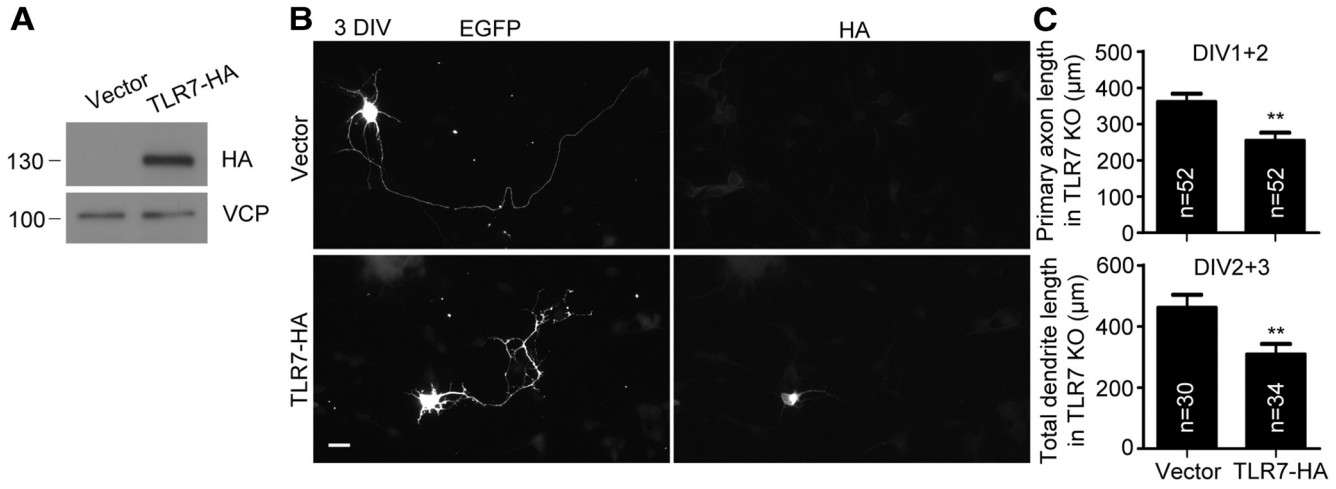

Figure 4. TLR7 overexpression rescues axonal and dendritic phenotypes in TLR7 KO cortical neurons. ***A***, Immunoblot of HEK cell extracts stained with HA tag antibody to analyze expression of the TLR7-HA construct. Transfection with vector alone was the negative control. VCP was an internal control. ***B***, Representative images of neurons cotransfected with EGFP and vector control and TLR7-HA, as indicated. ***C***, Quantitative data on axon and dendrite length. To analyze the axon length, the neurons were transfected with TLR7 at 1 DIV and fixed for immunostaining at 3 DIV. For the dendritic phenotype analysis, transfection was performed at 2 DIV and immunostaining was performed at 5 DIV. The data represent the mean + SEM. Scale bar, 20 μm. $^{**}p < 0.01$.

equipped with a 20× objective lens/numerical aperture (NA) 0.8 (Plan Apochromat; Carl Zeiss). Immunofluorescent images were captured with an AxioCam MRm digital camera driven by AxioVision digital image processing software at 20–22°C. The c-*fos* and MAP2-positive cortical neurons were visualized at 20–22°C with a confocal microscope (LSM 700; Carl Zeiss) equipped with a 20× objective lens/NA 0.8 (Plan Apochromat; Carl Zeiss). Images were captured with Zen acquisition and analysis software (Carl Zeiss). For publication, all of the images were processed with Photoshop (Adobe) with minimal adjustment of brightness or contrast applied to the whole images.

Immunoblotting. HEK293T cells were lysed and homogenized in RIPA buffer (150 mM NaCl, 50 mM Tris-HCl, pH 7.4, 1% Triton X-100, 0.25% sodium deoxycholate, 0.1% SDS, 2 mM EDTA and 1 mM PMSF) on ice for 30 min. After centrifugation at 13,000 rpm at 4°C for 20 min, the protein concentration of the supernatant was determined with a Bio-Rad protein assay kit. Equal amounts of proteins were separated by electrophoresis and then transferred to PVDF membranes (Milli-PROBE, Millipore) with 200 mA for 2 h at 4°C. The membranes were blocked with 5% nonfat milk in PBS for 1 h at room temperature and incubated with primary antibodies in blocking solution overnight at 4°C. After washing with PBS containing 0.1% Tween 20, membranes were incubated with HRP-conjugated secondary antibodies for 1 h at room temperature. Finally, the antibody-bound bands on the membranes were visualized by ECL Plus onto Fujifilm medical x-ray film.

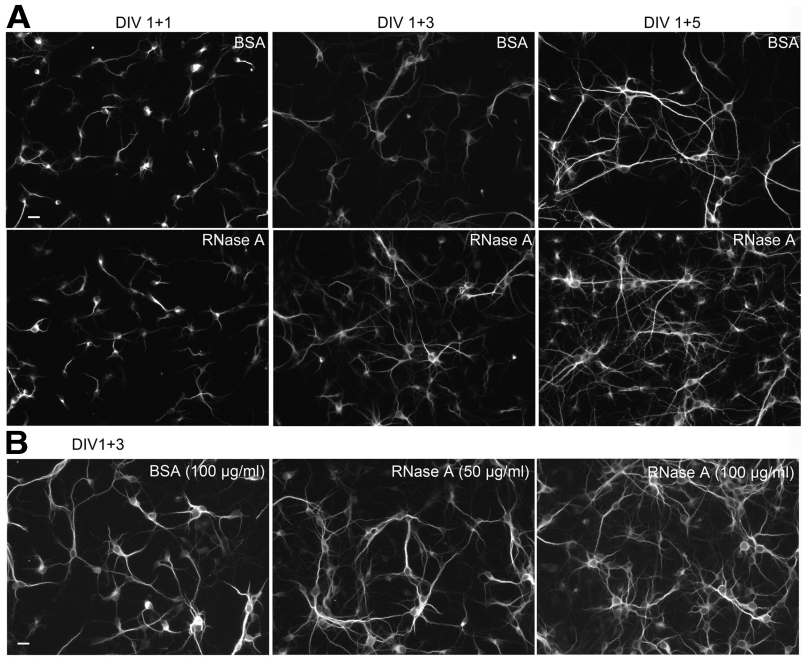

Figure 5. Treatment with RNase A promotes dendritic growth of cultured mouse cortical neurons. ***A***, Cultured neurons were treated with RNase A and BSA at a final concentration of 100 μg/ml for 1, 3, and 5 d. ***B***, Cultured neurons were treated with different concentrations of RNase A purchased from Invitrogen at 1 DIV and harvested for immunostaining at 4 DIV. Immunostaining with MAP2 antibody was performed to outline the dendrite morphology. Scale bars, 20 μm.

In utero *electroporation. In utero* electroporation was performed as described previously (Maiorano and Mallamaci, 2009; Zhao et al., 2009). Briefly, a pregnant ICR (CD-1) female was deeply anesthetized at E15.5 with ketamine (200 μg/g body weight) and xylazine (40 μg/g body weight). The uterine horns were then exposed by midline laparotomy. The plasmids that had been purified using an EndoFree Plasmid Maxi kit (Qiagen) were used at a final concentration of ~0.5–1 μg/μl mixed with 1% fast-green dye and injected into one of the lateral ventricles of an embryo using a glass micropipette with a sharp tip of ~0.1–0.2 mm in external diameter. Platinum tweezer-style circular electrodes (5 mm diameter) were then placed outside the uterus across the telencephalon of the embryo. Five pulses (30 V for 50 ms) at 950 ms intervals were applied using a BTX ECM830 square wave pulse generator (Genetronics). For each experiment, four to five electroporated offspring of either sex were anesthetized and perfused with 4% PFA in PBS at postnatal day 7 (P7), P14, or P21. After a 4% PFA postfixation overnight at 4°C and 30% sucrose dehydration, brains were embedded in OCT compound (Tissue-Tek; Sakura) and then sliced into 150-μm-thick sections using a cryostat and mounted on slides with mounting medium [1% DABCO (1,4-diazabicyclo[2.2.2]octane), 90% glycerol in PBS]. The morphology of layer 2/3 cortical neurons was visualized at 20–22°C with a confocal

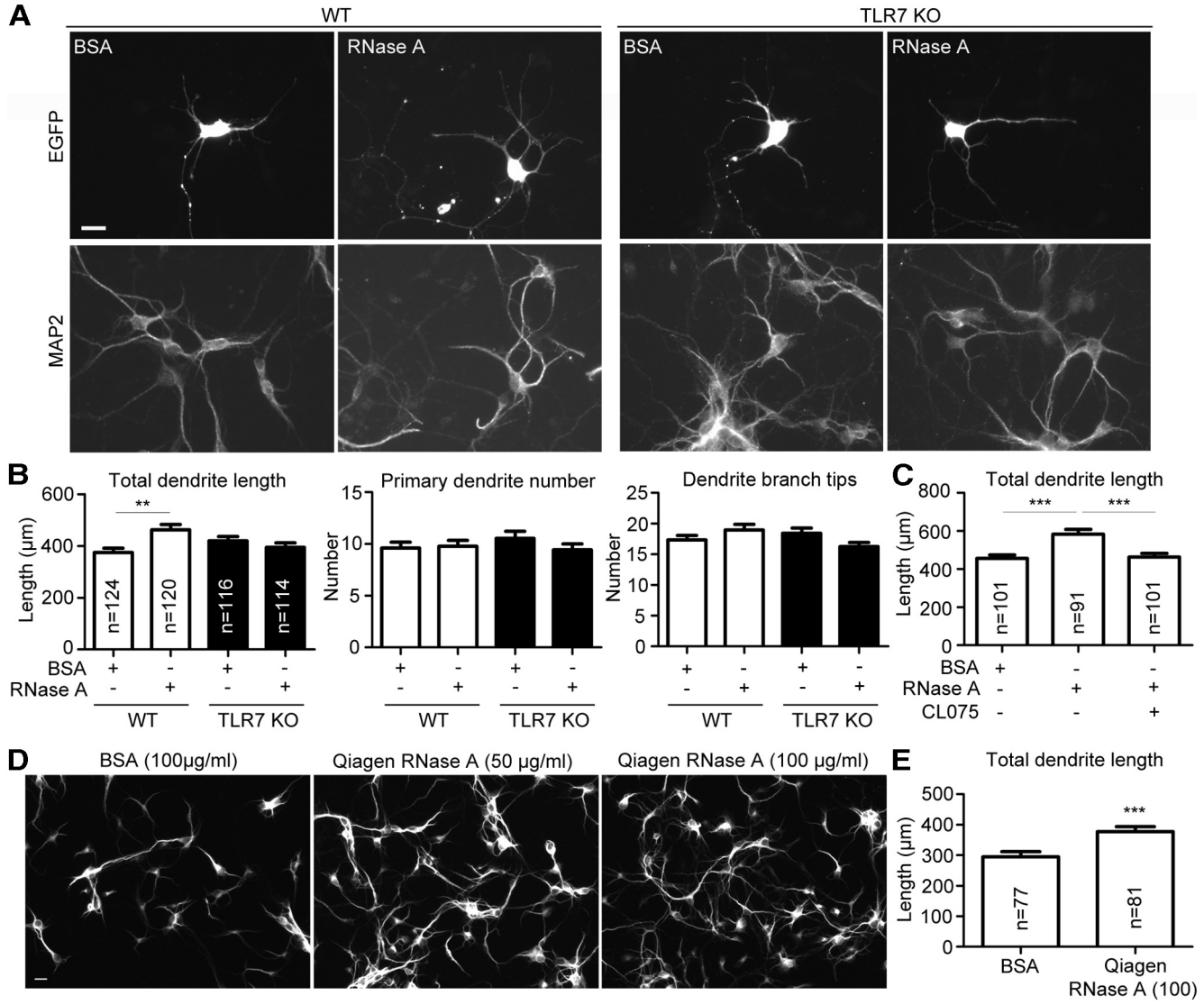

Figure 6. Removal of ssRNA from the cultures promotes dendritic growth. ***A***, RNase A treatment promotes dendrite growth in WT neurons but not TLR7 KO neurons. Cortical neurons were transfected with EGFP at 1 DIV, and RNase A (100 μg/ml) or BSA was added after transfection. The cultures were grown for 3 more days and subjected to immunostaining using EGFP and MAP2 antibodies. Scale bar, 20 μm. ***B***, Quantification of dendrite features in ***A***, including total dendrite length, primary dendrite number, and the number of dendrite branch tips. ***C***, CL075 (6 μM) was applied to RNase A-treated WT neurons at 3 DIV for 24 h. Dendrite length was then measured. ***D***, Cultured neurons were treated with different concentrations of RNase A purchased from Qiagen at 1 DIV and harvested for immunostaining at 4 DIV. Immunostaining with MAP2 antibody was performed to outline the dendrite morphology. Scale bar, 20 μm. ***E***, Quantification of ***D***. Neurons were collected from two or three independent experiments. Data represent the mean + SEM. $^{**}p < 0.01$; $^{***}p < 0.001$.

microscope (LSM 700; Carl Zeiss) equipped with a 40×/NA 1.25 objective lens (Plan Apochromat; Carl Zeiss). Images were captured with Zen acquisition and analysis software (Carl Zeiss).

Neuronal morphometry. To outline the cellular morphology, an EGFP construct was transfected alone or cotransfected with the indicated constructs into neurons. Dendrites and axons were identified with the dendritic marker MAP2 and the axonal marker SMI-312R. To determine the dendritic morphology, the following three parameters were measured: (1) the primary dendritic number, where the primary dendrites were defined as those MAP2-positive processes directly emerging from the soma; (2) the total dendrite length, including the length of all primary dendrites and dendritic branches; and (3) the number of dendritic branch tips, which represents the number of all dendritic branch ends. To analyze the primary axon length, the length of the longest processes emerging from soma with an SMI-312R-positive signal was measured. All images were analyzed using ImageJ software. Because the dendritic and axonal morphology of neurons is highly sensitive to culture conditions, particularly the quality of the B27 supplement, the same lot of B27 supplement was used when repeating each experiment. The data of the repeated experiments were then pooled for statistical analysis.

Open field test. The open field analysis was performed as described previously (Chung et al., 2011) with several modifications. For both WT and TLR7 KO mice, 10 mice of either sex were subjected to analysis at P11–P13. Locomotion and exploratory behaviors were measured in a new plastic box (28 × 20 × 14 cm). Each mouse was placed individually in the center of the box, and its movement was recorded from the top by videotaping for 3 min. The total distance moved and the speed were quantified with the Smart Video Tracking System (Panlab). The frequency of rearing (standing on hind legs) and time spent in rearing were counted manually.

Statistical analysis. Statistical analyses were performed using an unpaired Student's *t* test using GraphPad Prism, except for Figures 8, *A* and *B*, and 13, *B* and *C*. For Figure 8*A*, two-way ANOVA with Bonferroni's test performed using SigmaStat 3.5 was used. For Figures 8*B*, and 13, *B* and *C*, one-way ANOVA with Bonferroni's test by GraphPad Prism was used. Data are presented as the mean ± SEM or mean ± SD. For mor-

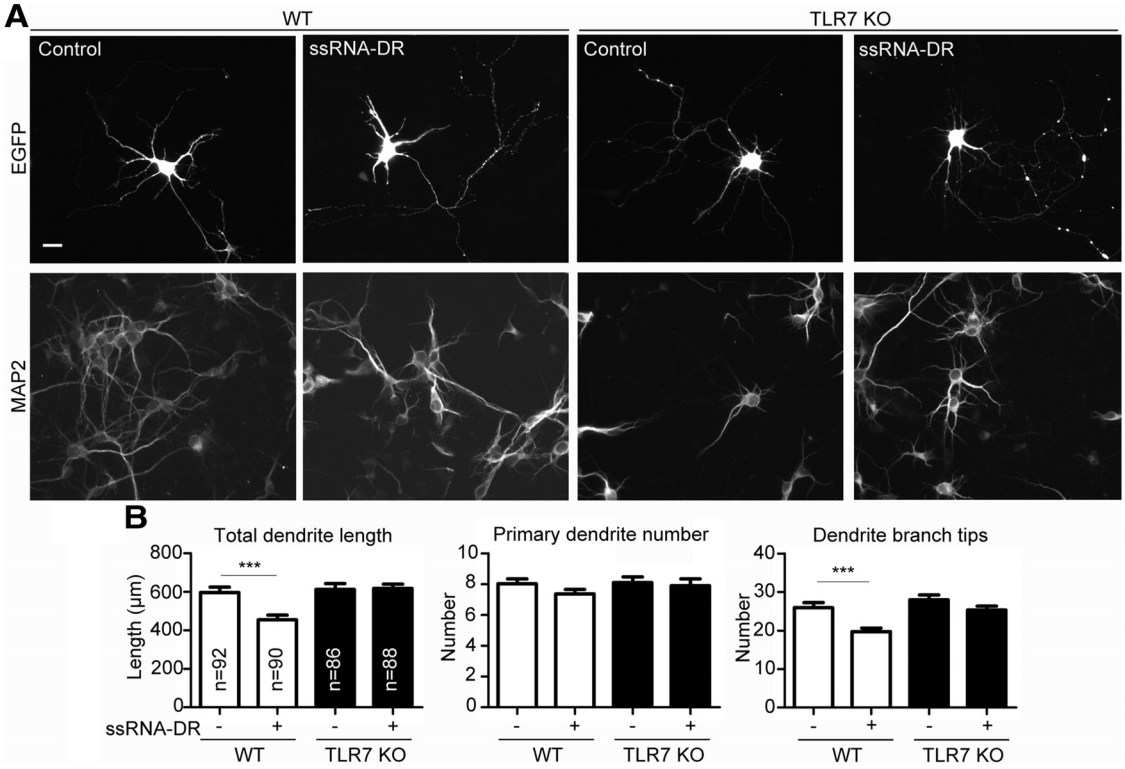

Figure 7. Addition of exogenous ssRNA impairs dendritic growth in WT but not in TLR7 KO neurons. ***A***, Cultured cortical neurons isolated from TLR7 KO mice and WT littermates were transfected with EGFP and treated with ssRNA-DR at 4 DIV at a final concentration of 5 μg/ml. One day later, the neurons were harvested for immunostaining using EGFP and MAP2 antibodies. Scale bar, 20 μm. ***B***, Quantification of ***A***. Neurons were collected from two independent experiments. Data represent the mean + SEM. ***$p < 0.001$.

phological studies, *n* indicates the number of neurons measured in each experiment.

Results

TLR7 agonist R837 impairs dendritic arborization of cultured cortical neurons

Previous studies indicated that TLR3 and TLR8 negatively regulate neurite outgrowth of dorsal root ganglion neurons and cortical cultured neurons (Ma et al., 2006; Cameron et al., 2007). In addition to neurite differentiation, our data showed that Sarm1, a TIR domain-containing adaptor, regulates dendritic arborization (Chen et al., 2011). We therefore wondered whether TLRs play a role in the regulation of dendrite outgrowth. To examine this possibility, TLR agonists were added into cultured mouse cortical neurons at 4 DIV. Dendritic arbors were then monitored 2 d later by immunostaining using dendrite marker MAP2. Among the examined agonists, we found that treatment with TLR7 agonist R837 reduced the dendrite length (Fig. 1). The rest of the agonists did not have any noticeable effects on dendrite growth (Fig. 1). We thus focused on TLR7 in the following experiments.

TLR7 but not TLR8 is the major TLR detecting ssRNA in the nervous system

We next confirmed the expression of TLR7 in cultured mouse cortical neurons using quantitative RT-PCR. TLR3, TLR4, and TLR8 were also examined. Normalized against an internal control, cyclophilin (Cyp), TLR3 and TLR7 transcripts were the two TLRs expressed most abundantly in cortical cultures (Fig. 2*A*), echoing the observations that activation of TLR7 and TLR3 impairs neuronal morphogenesis (Fig. 1; Cameron et al., 2007). TLR7 KO mice were used to confirm the specificity of our PCR conditions (Fig. 2*B*), supporting the reliability. Our data also echo the recent studies that demonstrated that TLR7 is expressed in developing and adult mouse brains at both the mRNA and protein levels (Kaul et al., 2012; Lehmann et al., 2012a).

Interestingly, we found that the numbers of TLR8 transcripts in TLR7 KO cortical neurons were increased compared with those detected in WT littermate neurons (Fig. 2*B*). As well as occurring in cultured cortical neurons, this compensation also occurs within the embryonic brain (Fig. 2*C*) but not in the embryonic liver (Fig. 2*D*), suggesting tissue specificity.

We further estimated the actual copy numbers of TLR7 and TLR8 in cultured neurons of WT littermates and TLR7 KO mice. In WT cultured neurons, there were 23.2 copies of the TLR7 transcript and only 2.1 copies of the TLR8 transcript in 1 ng of total RNA (Fig. 2*E*), meaning that TLR7 was ~11-fold more abundant than TLR8. The number of TLR8 transcripts was increased up to 15.4 copies/ng total RNA in TLR7 KO neurons at 4 DIV (Fig. 2*E*). These quantitative analyses further support the hypothesis that TLR8 compensates for TLR7 in TLR7 KO neurons, although the copy number of TLR8 in TLR7 KO neurons was still less than the copy number of TLR7 in WT neurons.

In conclusion, although both TLR7 and TLR8 recognize ssRNAs, the expression levels of TLR7 in the brain are much higher than those of TLR8, suggesting a more important role for TLR7 in neurons.

Deletion of TLR7 promotes dendritic and axonal growth in cortical neurons

To elucidate the function of TLR7 in neuronal morphology, we compared TLR7 KO and WT neurons. To minimize the variation, cultured neurons isolated from littermates were compared.

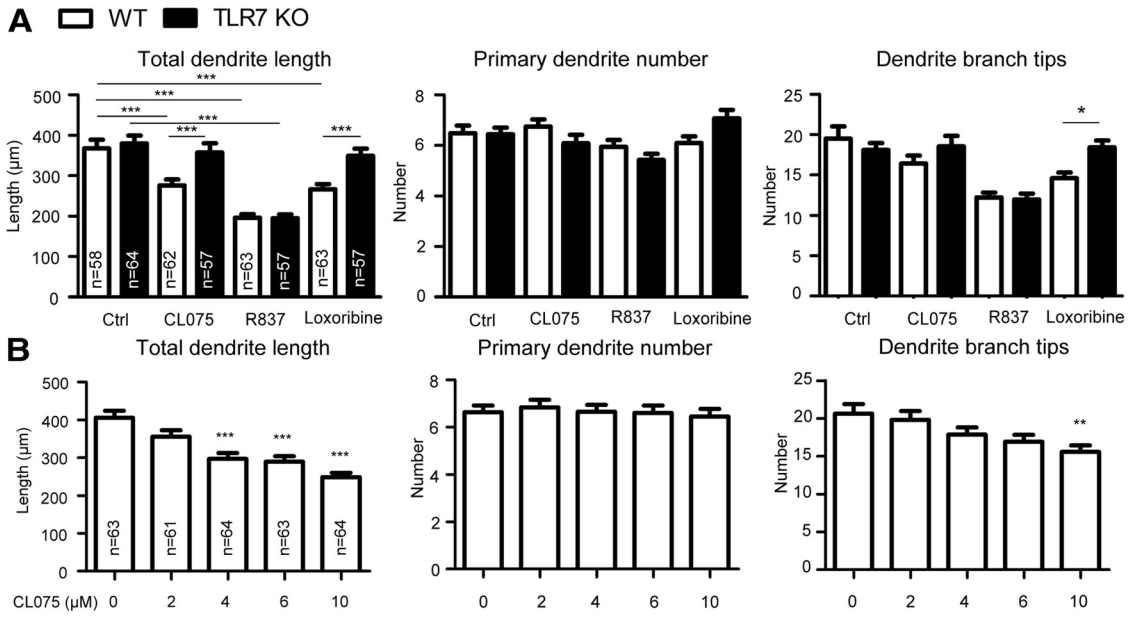

Figure 8. TLR7 activation with synthetic agonists restricts dendrite growth. ***A***, The effect of the different TLR7 agonists (6 μM CL075, 20 μM R837, 1 mM loxoribine) on total dendrite length, primary dendrite number, and the number of dendrite branch tips of WT and TLR7 KO cortical neurons were compared. Cortical neurons were transfected with EGFP at 1 DIV; the agonists were added to the cultures at 4 DIV. Neurons were then fixed for immunostaining using a MAP2 antibody 1 d later. Statistical analysis was performed using two-way ANOVA with Bonferroni's test. ***B***, The dosage effect of CL075 on dendrite morphology of WT neurons. One-way ANOVA analysis was used to compare the difference. Data represent the mean + SEM. $*p < 0.05$; $**p < 0.01$; $***p < 0.001$. Ctrl, Control.

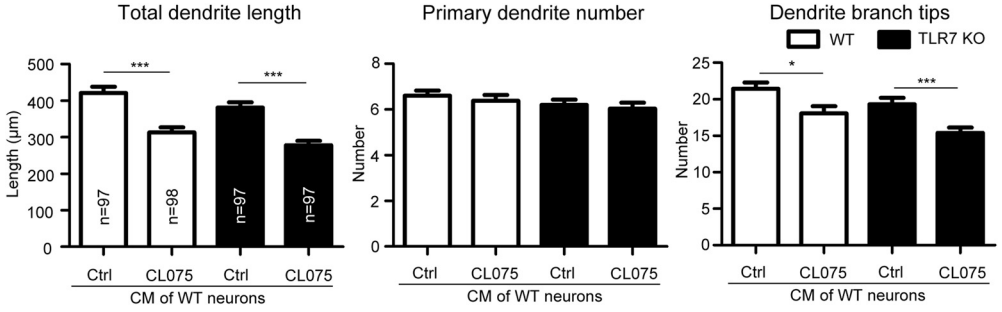

Figure 9. The conditioned medium of CL075-treated wild-type neurons restricts dendrite growth of WT as well as TLR7 KO cortical neurons. CL075 (6 μM) was added to the WT cortical neurons at 3 DIV. One day later, the conditioned medium (CM) was harvested and added to new WT and TLR7 KO cultures at 4 DIV. Transfection of EGFP was performed at 1 DIV, and immunostaining was performed at 5 DIV. Data represent the mean + SEM. $*p < 0.05$; $***p < 0.001$. Ctrl, Control.

Neurons were transfected with an EGFP expression construct at 1 DIV to outline individual axons and dendrites. Double staining with dendritic marker MAP2 was performed to identify dendrites (data not shown). The total dendritic length, and the numbers of primary dendrites and dendritic branch tips were measured at 5 and 7 DIV. At 5 DIV, no noticeable difference could be seen between WT and TLR7 KO neurons (Fig. 3*A*). However, at 7 DIV, the total dendritic length and the total number of dendritic tips were significantly increased in TLR7 KO neurons (Fig. 3*A*), supporting the role of TLR7 in negative regulation of dendrite extension.

We also investigated whether TLR7 influences axon growth. The axonal lengths of WT and TLR7 KO cortical neurons were compared at 2, 3, and 4 DIV. The primary axon length of TLR7 KO neurons was longer than those of WT neurons at 2 and 3 DIV (Fig. 3*B*). However, at 4 DIV, there was no obvious difference between WT and TLR7 KO neurons (Fig. 3*B*). We noticed that, from 3 to 4 DIV, WT neurons still effectively extended their axons; however, TLR7 KO neurons showed very limited axonal extension during this period (Fig. 3*B*). Together, these results indicate that TLR7 restricts the growth of both axons and dendrites within critical time windows in neuronal cultures; however, it is not clear what factors define this critical window. It is possible that the expression level and subcellular distribution of the receptor itself and the presence of ligands influences the outcomes.

To confirm that axon and dendrite outgrowth of TLR7 KO neurons is indeed caused by TLR7 deletion, a rescue experiment was performed by transfecting exogenous HA-tagged TLR7 into TLR7 KO neurons. The expression of exogenous TLR7 was monitored by HA tag antibody (Fig. 4*A*,*B*). Compared with the vector control, TLR7 expression shortened the length of both axons and dendrites in TLR7 KO neurons (Fig. 4*B*,*C*), suggesting the specificity of TLR7 on the restriction of axonal and dendrite growth.

Single-stranded RNAs in culture regulate dendrite growth

In the above data, an increase or reduction in TLR7 expression in cultured neurons was sufficient to influence dendrite and axon growth, suggesting the presence of ligands for TLR7 in the cultures. In addition to ssRNA derived from pathogens, TLR7 also

interacts with endogenous mRNA and miRNA (Barrat et al., 2005; Lau et al., 2005; Diebold et al., 2006; Lehmann et al., 2012a). It is likely that ssRNAs released from dead cells or exosomal miRNA in the culture activate TLR7. We applied RNase A to examine this hypothesis. Because RNase A is ready to be internalized through clathrin-mediated endocytosis and macropinocytosis (Chao and Raines, 2011), RNase A can digest ssRNA not only in the supernatant but also in the intracellular vesicles. A concentration of 100 μg/ml RNase A (Invitrogen) was added to the cultures at 1 DIV for 1, 3, and 5 d; BSA was used as a control. A 1 d treatment of RNase A had no noticeable effect on dendritic arborization (Fig. 5*A*), while RNase A treatment for 3 d promoted dendritic growth (Fig. 5*A*). The effect of a 5 d treatment was even more dramatic (Fig. 5*A*). We also added different doses of RNase A to cultures at 1 DIV and examined the effects at 4 DIV. Indeed, a higher concentration of RNase A resulted in better dendritic growth, as the MAP2-positive processes were more complex in cultures treated with higher amounts of RNase A (Fig. 5*B*).

To quantify the effects of RNase A on dendritic morphology, we used EGFP to outline neuronal morphology and examined the effect of 100 μg/ml RNase A treatment for 3 d. In WT neurons, RNase A treatment increased total dendrite length (Fig. 6*A*,*B*). In contrast, TLR7 KO neurons did not respond to RNase A treatment (Fig. 6*A*,*B*), suggesting a specific role of TLR7 in the response to RNase A treatment. To confirm that RNase A treatment does not harm TLR7 per se, we applied CL075 (3M002), a thiazoloquinolone compound, to RNase A-treated neurons. CL075 has been shown to activate murine TLR7 (Gorden et al., 2005, 2006a,b). We found that CL075 still reduced the total dendrite length of RNase A-treated neurons (Fig. 6*C*), suggesting that RNase A treatment removes the ligands but does not impair TLR7.

In addition to RNase A purchased from Invitrogen, we also tried RNase A ordered from Qiagen. Basically, RNase A obtained from Qiagen also promoted dendrite growth and resulted in longer dendrites of cultured cortical neurons (Fig. 6*D*,*E*). In conclusion, our data suggest that RNase A treatment facilitates dendrite growth and that TLR7 is involved in the process.

To further confirm that TLR7 activation by ssRNA impairs dendrite growth, ssRNA-DR, a short ssRNA recognized by

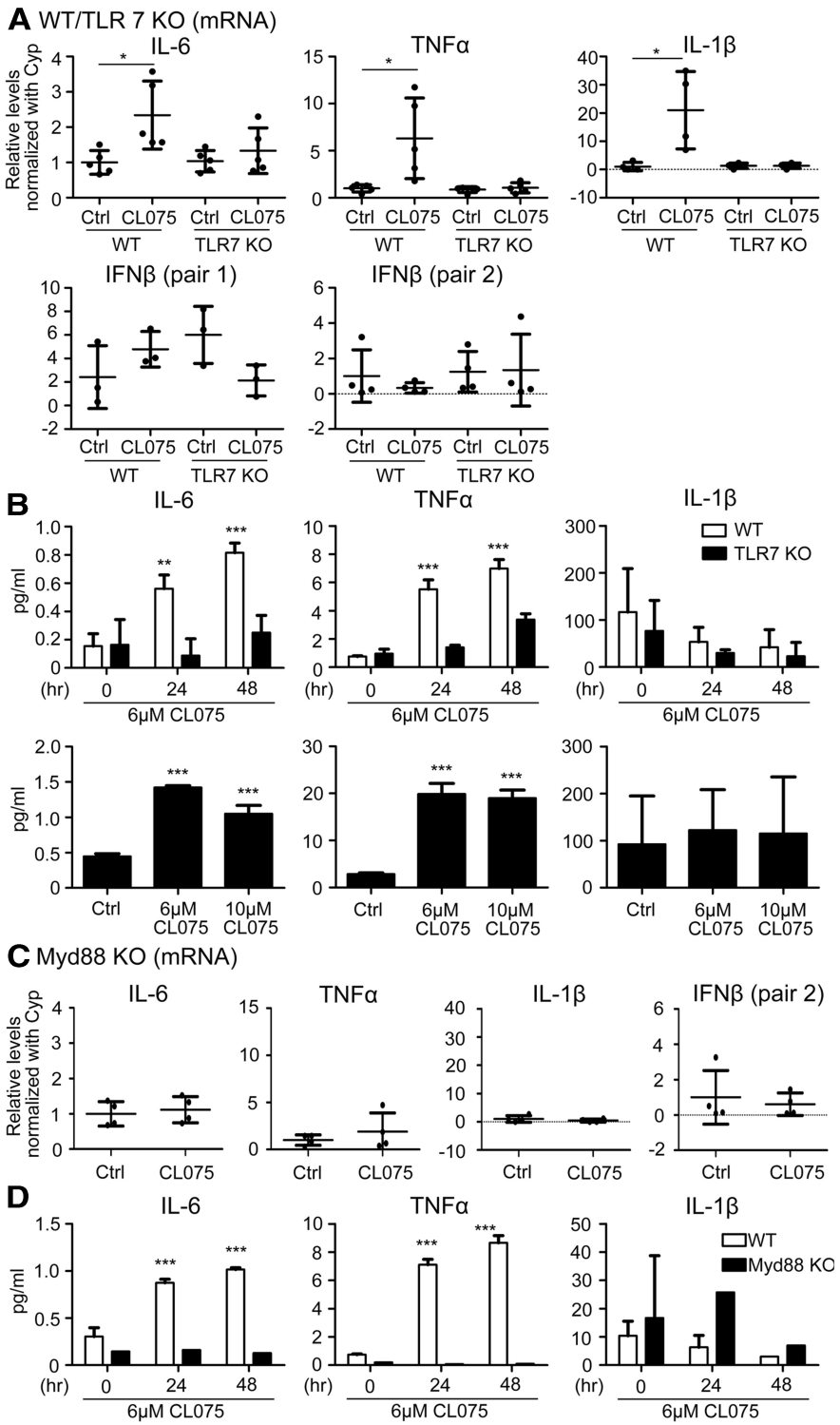

Figure 10. TLR7 activation induces IL-6 and TNF-α expression in cultured neurons. ***A***, ***C***, Real-time PCR to quantify cytokine expression upon TLR7 activation. Cultured cortical neurons of WT and TLR7 KO mice (***A***) and Myd88 KO mice (***C***) were treated with CL075 (4 μM) and vehicle for 6 h and harvested for real-time PCR using Cyp as an internal control (Ctrl) to quantify the relative mRNA levels of IL-6, TNF-α, IL-1β, and IFN-β at 4 DIV. For IFN-β, two pairs of primers were used. Neither of these two pairs of primers detected noticeable induction of IFN-β expression. ***B***, ***D***, ELISA to detect cytokine proteins in the supernatants of cultures. The culture supernatants of WT, TLR7 KO, and Myd88 KO neurons were collected to detect the presence of IL-6, TNF-α, and IL-1β at 24 and 48 h after stimulation with different concentrations of CL075 and vehicle control, as indicated. Data represent the means $\pm$ SD in ***A*** and ***C***, and the means + SD in ***B*** and ***D***. $^{*}p < 0.05$; $^{**}p < 0.005$; $^{***}p < 0.001$.

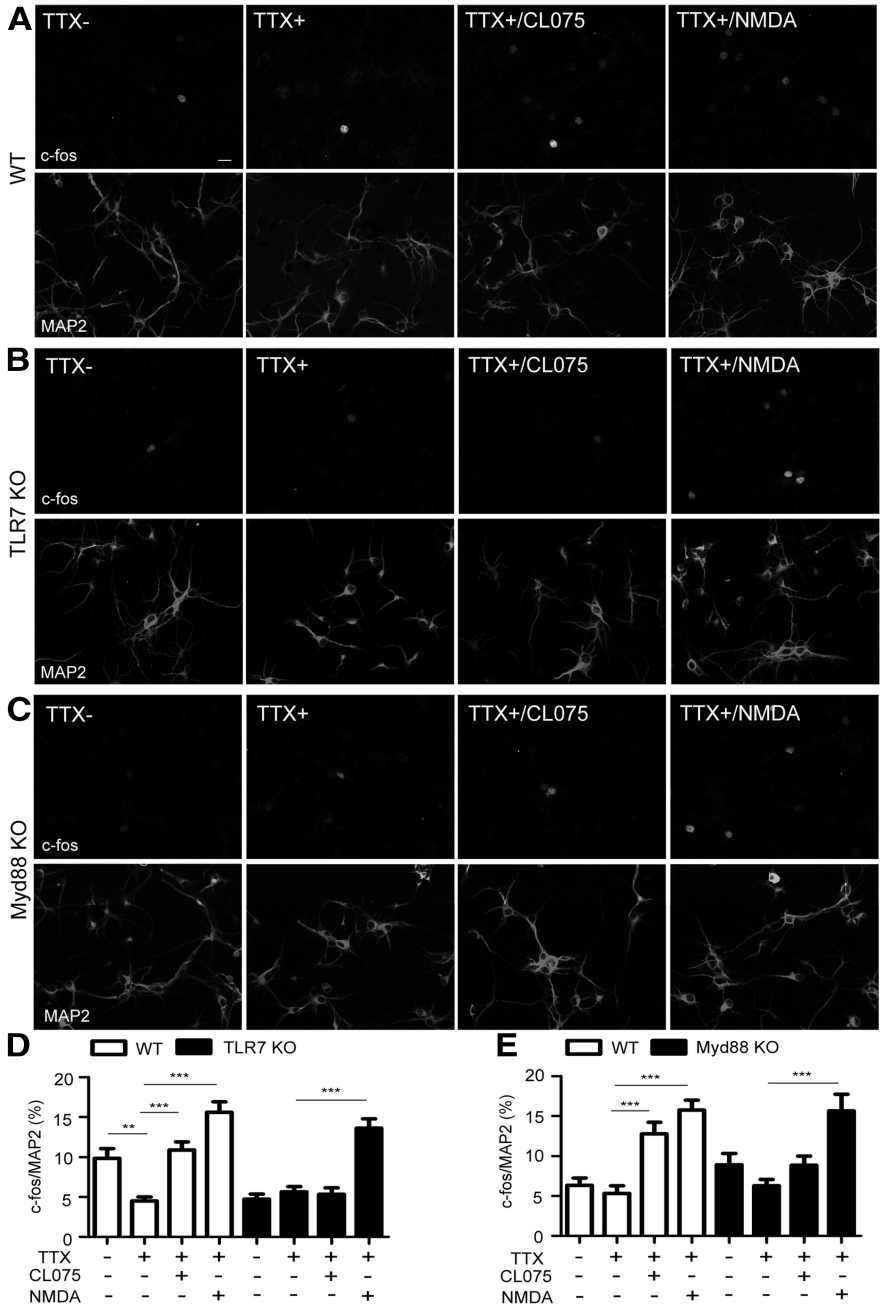

Figure 11. c-Fos proteins are induced by TLR7 activation in cultured neurons. ***A–C***, Immunostaining with c-Fos and MAP2 antibodies. Cultured cortical neurons of WT (***A***), TLR7 KO (***B***), and Myd88 KO (***C***) mice were pretreated with TTX (1 μM) for 30 min, and further activated with CL075 (6 μM) and NMDA (10 μM) for 4 h at 4 DIV. Neurons were then fixed for immunostaining. Scale bar, 20 μm. ***D***, ***E***, Quantitative analyses of c-Fos-positive neurons. The data were compared between littermates and KO mice. Neurons were collected from more than three independent experiments. About 10 images were taken in each experiment. Data represent the mean + SEM. $^{**}p < 0.01$; $^{***}p < 0.001$.

mouse TLR7 (Hornung et al., 2005), was added to cultured mouse cortical neurons at 4 DIV. Cells were then harvested for immunostaining at 5 DIV. Compared with the vehicle control, ssRNA-DR noticeably reduced the total dendritic length and the number of dendritic branch tips of WT neurons (Fig. 7*A*,*B*). The addition of ssRNA-DR did not impair dendritic growth in TLR7 KO neurons (Fig. 7*A*,*B*). These results suggest a negative role for ssRNA in the regulation of the dendritic growth of neurons that acts via TLR7.

TLR7 activation restricts dendrite growth in neuronal cultures

To further investigate the role of TLR7 in neurons, the effects of three TLR7 agonists, CL075, R837, and loxoribine, on dendrite growth were examined. In WT neurons, treatment with CL075, R837, and loxoribine all resulted in shorter total dendrite lengths (Fig. 8*A*). To confirm the specificity, these TLR7 agonists were also added into TLR7 KO neurons. We found that neither CL075 nor loxoribine impaired dendritic arborization of TLR7 KO neurons (Fig. 8*A*), suggesting the specificity of CL075 and loxoribine in the activation of TLR7. In contrast, R837 treatment still efficiently reduced the total dendrite length and the number of dendritic branch tips of TLR7 KO neurons (Fig. 8*A*), indicating that the negative effect of R837 on dendritic arborization is not mediated by TLR7 activation. We further examined the dosage effect of CL075 on dendritic arborization. Indeed, CL075 reduced the total dendrite length and the number of dendritic branch tips in a dosage-dependent manner within a concentration range of 2–10 μM (Fig. 8*B*). Together, these results suggest that CL075 and loxoribine, but not R837, specifically activate TLR7 and result in smaller dendrite arbors of cultured cortical neurons.

Factors secreted by TLR7-activated cells downregulate dendrite growth

We then wondered how TLR7 regulates neuronal morphology. Because IL-6, IL-1β, and TNF-α, the well characterized downstream effectors of TLR7 in the innate immune response, have also been shown to downregulate dendrite development of cultured cortical neurons (Gilmore et al., 2004), we investigated the possibility that TLR7 induces cytokine expression and restricts dendrite growth. If this hypothesis was correct, we would expect that secreted factors in the culture medium of CL075-treated neurons should be able to impair dendrite growth. To test this possibility, the conditioned medium from the WT neuronal cultures treated with CL075 or vehicle control was collected and added to naive WT cortical neurons. We found that the conditioned medium of CL075-treated neurons reduced the total dendrite length and the number of dendritic tips of WT neurons (Fig. 9). However, it is not clear whether there was any residual CL075 in the conditioned medium, which may have still been able to activate TLR7 and inhibit dendrite growth in the treated cultures. To rule out the effect of CL075, we applied the conditioned medium to TLR7 KO neurons, which did not respond to CL075 stimulation (Fig. 8*A*). The result showed that the CL075-treated conditioned medium still effectively repressed dendrite growth of TLR7 KO neurons

(Fig. 9). These results indicate that TLR7 activation induces secretion of some factors, which leads to the restriction of dendrite growth.

TLR7 activation in neurons induces IL-6 and TNF-α expression through Myd88

We then examined the involvement of cytokines in TLR7-regulated dendritic growth. Using quantitative RT-PCR analysis, we first found that the RNA expression levels of inflammatory cytokines IL-6, TNF-α, and IL-1β were increased after CL075 treatment in WT neurons (Fig. 10*A*, top). In contrast, the antiviral cytokine IFN-β was not induced by CL075 (Fig. 10*A*, bottom). Since a previous study showed that intracerebroventricular injection of CL075 induced IFN-β expression in brain (Butchi et al., 2008), we were concerned about whether the detection of IFN-β by our primers was less efficient. To rule out this possibility, a new set of primers was designed for real-time PCR. However, with the new set of primers, the induction of IFN-β expression was still undetected (Fig. 10*A*, bottom), suggesting that TLR7 activation did not induce IFN-β expression in cultured cortical neurons. In TLR7 KO neurons, CL075 treatment did not induce IL-6, TNF-α, and IL-1β expression (Fig. 10*A*), indicating the specificity. These results suggest that TLR7 activation in cultured neurons induces RNA expression of inflammatory cytokines IL-6, TNF-α, and IL-1β, but not antiviral cytokine IFN-β.

In addition to the mRNA levels, the protein levels of IL-6, TNF-α, and IL-1β were also measured in the culture supernatants. After CL075 treatment, a time-dependent increase in both IL-6 and TNF-α proteins was found in the supernatants (Fig. 10*B*). The dosage effect from 6 to 10 μM was not clear. Perhaps the response had already reached a plateau at 6 μM CL075. In contrast to IL-6 and TNF-α, the protein levels of IL-1β in the supernatants showed no noticeable increase after CL075 stimulation for 24 and 48 h (Fig. 10*B*). Since pro-IL-1β needs to be processed by active caspase-1 to produce and secrete active IL-1β, and since caspase-1 activated by the inflammasome requires a second signal (Mariathasan and Monack, 2007), the sole signal from TLR7 in cultured neurons is probably not sufficient to activate the inflammasome, and it is thus unable to process pro-IL-1β and secrete IL-1β into the supernatant. These data suggest the IL-6 and TNF-α are the two major downstream effectors of TLR7 in cultured cortical neurons.

Since Myd88 is the key TIR domain-containing adaptor for TLR7 in innate immune response, we then wondered whether Myd88 is required for the activation of IL-6 and TNF-α expression by TLR7. To investigate this possibility, Myd88 KO cortical neurons were cultured and their response to CL075 was examined. None of the IL-6, IL-1β, TNF-α and IFN-β was induced by CL075 treatment in Myd88 KO neurons (Fig. 10*C*,*D*), indicating that Myd88 is required for TLR7-induced cytokine expression in neurons.

c-Fos proteins are induced by TLR7 activation in cultured neurons

To induce the expression of inflammatory cytokines, Myd88 delivers the signal to activate AP-1 and NF-κB transcription factors. We wondered whether this classical signal pathway is also conserved in cultured cortical neurons. To address this possibility, expression of c-Fos, a critical AP-1 member in neurons, was examined after CL075 treatment. Because neuronal activation also induces c-Fos expression, cultured neurons were pretreated with TTX to reduce neuronal activity and stimulated with CL075. Immunostaining with c-Fos antibody indicated that c-Fos expression was induced in WT neurons after CL075 stimulation (Fig. 11*A*,*D*,*E*). This induction was dependent on TLR7 and Myd88 because the upregulation of c-Fos expression was not found in either TLR7 or Myd88 KO neurons (Fig. 11*B*–*E*). To further confirm that the unresponsiveness of c-Fos to CL075 stimulation is specifically due to deletion of TLR7 and Myd88 but not failure of c-Fos expression, we stimulated cultured cortical neurons with NMDA. We found that, similar to WT neurons, TLR7 and Myd88 KO neurons also increased c-Fos expression in response to NMDA stimulation.

Together, these results suggest that TLR7 activation in neurons likely uses the classical innate immune response signaling pathway to induce the expression of inflammatory cytokines.

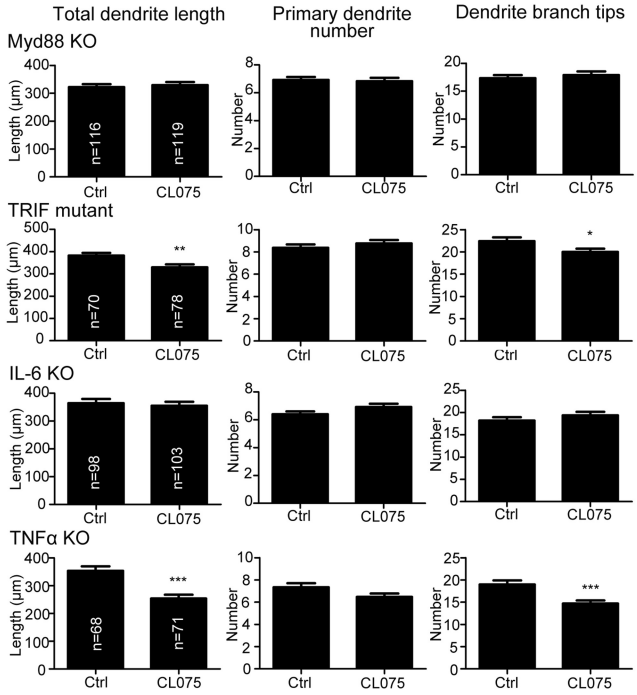

Figure 12. TLR7 negatively regulates dendritic growth through the Myd88 –IL-6 pathway. CL075 (6 μM) was added to the Myd88 KO, TRIF mutant, IL-6 KO, and TNF-α KO cultures at 4 DIV for 24 h. The total dendrite length, primary dendrite number, and the number of dendrite branch tips were measured. Myd88 and IL-6 KO cortical neurons did not respond to CL075. Experiments were repeated at least three times. Data represent the mean + SEM. $*p < 0.05$; $**p < 0.01$; $***p < 0.001$. Ctrl, Control.

IL-6 and Myd88 mediate the negative role of TLR7 in dendrite growth

We then used knock-out mice to investigate whether Myd88, IL-6, and TNF-α are required for TLR7-induced downregulation of dendrite growth. If these factors are critical for TLR7 in the restriction of dendrite growth, deletion of the genes encoding these proteins should impair the response of cultured neurons to CL075. CL075 treatment did not reduce the total dendrite length, primary dendrite number, or the number of dendrite branch tips of Myd88 KO and IL-6 KO neurons (Fig. 12). However, TNF-α KO neurons did respond to CL075 treatment (Fig. 12). These results support the notion that Myd88 and IL-6, but not TNF-α, are essential for TLR7-mediated dendritic withdrawal. To confirm the specific roles of Myd88 and IL-6 in response to TLR7 activation, we also examined the effect of CL075 on dendrite growth of TRIF mutant neurons, which carry a single base pair deletion in the TRIF gene induced by chemical mutagenesis

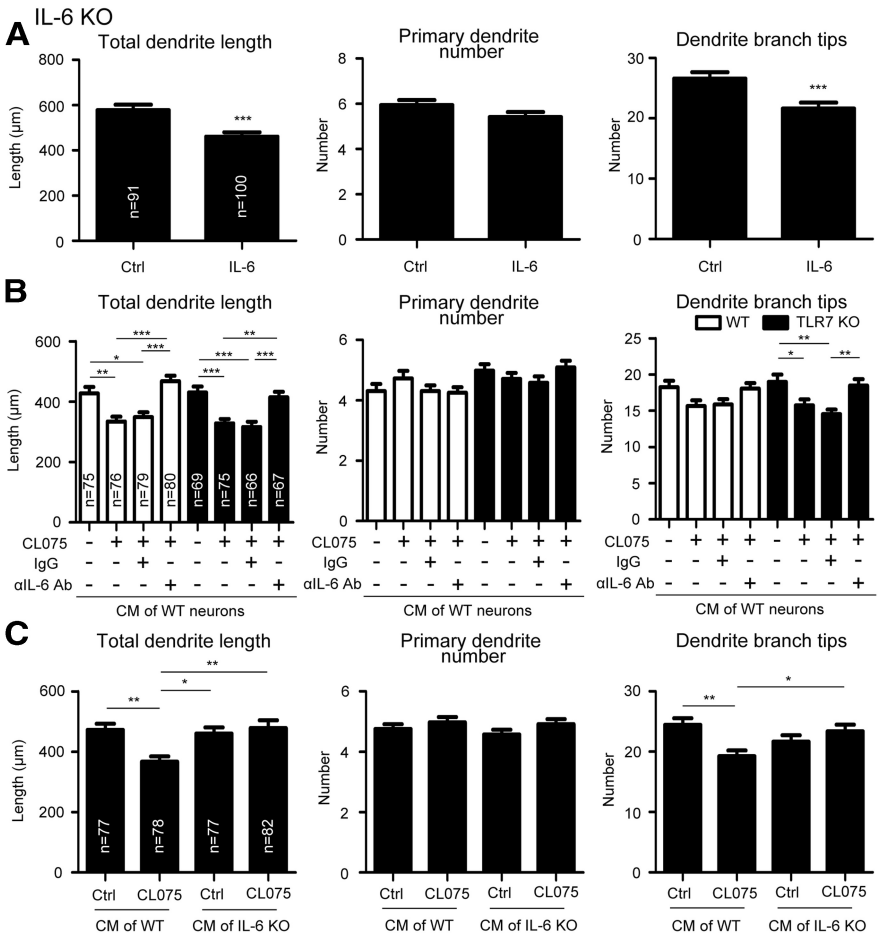

Figure 13. IL-6 restricts dendritic growth in cultured neurons. ***A***, Morphometric analysis of IL-6 KO neurons treated with 1000 U of recombinant IL-6 at 4 DIV for 24 h. ***B***, IL-6 neutralizing antibody diminishes the inhibitory effect of CL075-treated conditioned medium (CM) on dendrite growth. CL075 (6 μM) or vehicle control (Ctrl) was added to the WT cortical neurons at 3 DIV. One day later, CM was collected and mixed with IL-6 neutralizing antibody or isotype control antibody (IgG) at a concentration of 50 μg/ml and then added to WT and TLR7 KO neurons at 4 DIV for 24 h. ***C***, CL075-treated CM of IL-6 KO neurons does not inhibit dendrite growth of WT neurons. WT and IL-6 KO neurons were treated with CL075 (6 μM) for 4 h at 3 DIV. After washing with PBS, neurons were incubated in new media for 1 more day. The conditioned medium was then harvested and added to WT neurons at 4 DIV for 24 h. Total dendrite length, primary dendrite number, and the number of dendrite branch tips were measured. ***B***, ***C***, One-way ANOVA analysis was performed for statistical analysis. Data represent the mean + SEM. $*p < 0.05$; $**p < 0.01$; $***p < 0.001$.

(Hoebe et al., 2003). TRIF is the TIR domain-containing adaptor specific for TLR3 and TLR4, but not TLR7 or other Myd88-dependent TLRs. After CL075 stimulation, the total dendrite length and the number of dendrite branch tips of TRIF mutant neurons were still reduced (Fig. 12), suggesting that TRIF is not essential for restriction of dendrite growth by TLR7. Together, our results indicate that the downregulation of dendrite growth by TLR7 is mediated by the Myd88–IL-6 pathway.

The results above demonstrated that although both IL-6 and TNF-α are induced by TLR7 activation, only IL-6 is required for TLR7-mediated dendritic withdrawal. To further investigate the unique role of IL-6 in the TLR7 pathway, we performed three further experiments. The first experiment monitored the effect of exogenous IL-6 on cultured neurons. Mirroring a previous study using WT neurons (Gilmore et al., 2004), exogenous IL-6 shortened the total dendrite length of IL-6 KO neurons (Fig. 13*A*). The second experiment was to block the function of IL-6 using IL-6 neutralizing antibody. The conditioned medium of CL075-treated WT neurons was mixed with IL-6 neutralizing antibody and then added to both WT and TLR7 KO neurons. The presence of IL-6 neutralizing antibody completely blocked the negative effect of the conditioned medium on the dendrite growth of both WT and TLR7 KO mice (Fig. 13*B*). The effect was specific because control IgG did not influence the dendrite growth (Fig. 13*B*). To further confirm that IL-6 is essential for the effect of TLR7 on dendrite withdrawal, conditioned media of CL075-treated WT and IL-6 KO neurons were applied to WT cultured neurons. The conditioned medium collected from IL-6 KO neurons did not restrict dendrite growth (Fig. 13*C*), giving further credence to the essential role of IL-6 in TLR7-mediated dendrite withdrawal.

Reduction of TLR7 impairs dendrite growth in mouse brains

In addition to the *in vitro* studies, we further explored the role of TLR7 *in vivo*. Two artificial miRNA expression plasmids, miR-TLR7#1 and #2, were generated to knock down TLR7 expression. A control construct, miR-Ctrl, that expresses an artificial miRNA predicted to not target any mammalian gene was included. The artificial miRNAs were inserted into the 3′ untranslated region of an EGFP transcript, and thus the EGFP signal was used to indicate the expression of artificial miRNA and to outline cell morphology. Compared with miR-Ctrl, both miR-TLR7#1 and #2 reduced the level of HA-tagged TLR7 protein in HEK293 cells (Fig. 14*A*). The knockdown efficiency in cultured neurons was also examined. HA-tagged TLR7 was cotransfected with miR-TLR7#1 into cultured cortical neurons. Immunostaining with HA tag antibody was performed to quantify the expression of HA-tagged TLR7 in individual transfected neurons. We found that miR-TLR7#1 also reduced the expression of HA-tagged TLR7 in cortical neurons (Fig. 14*B*).

To evaluate the function of TLR7 *in vivo*, we then used IUE to knock down TLR7 in cerebral cortex. Because the CMV promoter does not efficiently drive the expression of exogenous genes in IUE experiments (Tabata and Nakajima, 2008), the miRNA cassettes of miR-TLR7#1 and miR-Ctrl were then subcloned into the vector pCAG-GFP. In HEK293T cells, pCAG-GFP-miR-TLR7#1 still effectively reduced HA-tagged TLR7 expression (Fig. 14*C*). The constructs pCAG-GFP-miR-Ctrl and pCAG-GFP-miR-TLR7#1 were then electroporated into the mouse embryonic cortex at E15.5. Dendritic arborization of transfected layer 2/3 cortical neurons was analyzed after birth. We found that the dendritic arbors of the TLR7 knock-down neurons were more complicated at P7, as they showed longer total dendritic length and more dendritic branch tips (Fig. 14*D*,*E*). In addition to P7, we further examined the effects of TLR7 knockdown at P14 and P21. At P14, TLR7 knockdown continued to result in more complex dendritic arbors (Fig. 14*E*). Unexpectedly, there were no noticeable differences between the TLR7 knock-down and control neu-

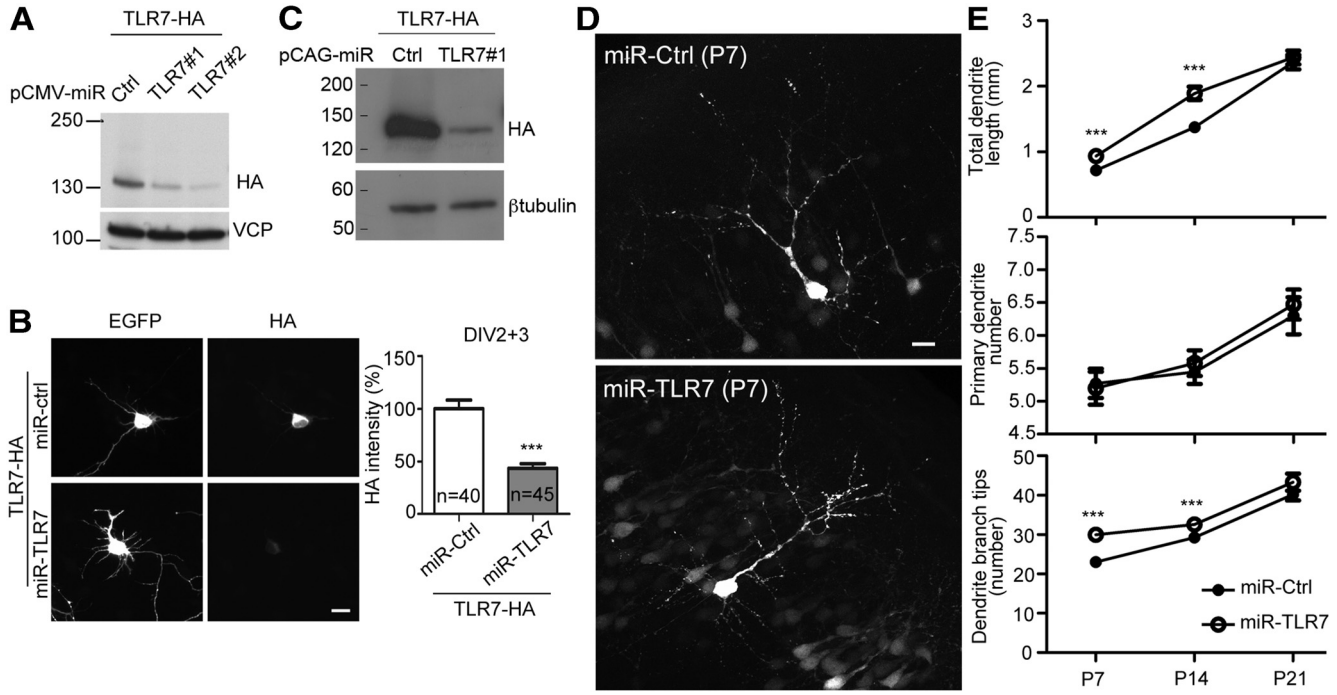

Figure 14. Knockdown of TLR7 promotes dendritic arborization *in vivo*. ***A***, The knock-down effects of two different TLR7 miRNA constructs on cotransfected HA-tagged TLR7 in HEK293T cells. VCP was used as an internal control (Ctrl). ***B***, The miR-TLR7#1 construct reduced the expression of cotransfected HA-tagged TLR7 in cultured cortical neurons as determined by immunostaining with an HA tag antibody. ***C***, Knock-down efficiency of pCAG-GFP-miR-TLR7#1 in HEK293T cells. β-Tubulin was used as an internal control. ***D***, Knockdown of TLR7 *in vivo* promoted dendritic arborization of layer 2/3 cortical neurons at P7. ***E***, Quantitative analyses of the effect of TLR7 knockdown on dendrites. For P7: miR-ctrl, a total of 28 neurons from five mice; miR-TLR7, a total of 30 neurons from four mice. For P14: miR-ctrl, a total of 24 neurons from four mice; miR-TLR7, a total of 24 neurons from four mice. For P21: miR-ctrl, a total of 22 neurons from four mice; miR-TLR7, a total of 22 neurons from four mice. For ***D*** and ***E***, *in utero* electroporation was performed at E15.5 to transfect pCAG-GFP-miR-ctrl and -miR-TLR7#1 into the cerebral cortices of ICR mice. Scale bar, 20 μm. The data represent the mean ± SEM. ***$p < 0.001$.

rons at P21 (Fig. 14*E*). These *in vivo* analyses indicate that the reduction in TLR7 expression within neurons promotes dendritic growth at early postnatal stages, such as at P7 or P14; however, the effects of the knockdown of TLR7 on neuronal morphology are diminished when neural development is more complete at P21 (Fig. 14*E*).

In conclusion, this evidence supports the *in vivo* function of TLR7 in regulation of dendrite morphogenesis. TLR7 likely plays a more important role during the developmental stage but not the stage when neural development is complete.

Juvenile TLR7 knock-out mice exhibit less exploratory activity in an open field

We then wondered whether reduction of TLR7 has any impact on mouse behavior. Since the morphological differences were seen before mice were 3 weeks old, we here focused on analyses using juvenile mice. We first monitored the body weight of TLR7 KO mice and WT littermates and found that they were comparable (Fig. 15*A*). The dates of eye opening were also recorded. Both TLR7 KO mice and WT littermates opened their eyes around P13 or P14 (Fig. 15*B*). The locomotor activity of mice was then measured every day in an open field from P9 to P14. The total distances moved and the speed of movement were also comparable in TLR7 KO mice and WT littermates (Fig. 15*C*). However, TLR7 KO mice displayed less on-wall rearing activity between P11 and P13 (Fig. 15*C*). Both the total number of rears and time spent in rearing were higher in WT littermates than TLR7 KO mice (Fig. 15*C*). These results suggest that in addition to neuronal morphology, TLR7 knockout also influences the exploratory activity of mice.

Discussion

Physiological significance of TLR7 in neurons

In this report, we provide evidence that TLR7 is expressed in murine cortical neurons and regulates dendritic growth in response to ssRNA. It is reasonable to speculate that during neuronal development, the expression of TLR7 ensures that neurons have the ability to detect ssRNAs that represent danger signals, possibly preventing their growth into areas of viral infection and/or cell death. Interestingly, it has been suggested that prenatal infections, such as influenza viral infection, influence neural development and induce psychiatric disorders such as schizophrenia and autism (Brown et al., 2000; Patterson, 2002, 2009). Maternal cytokines have been suggested to play a critical role in mediating the effects of prenatal infection on neural development (Brown et al., 2000; Patterson, 2002, 2009). The evidence in this report also supports the possibility that the innate immunity of neurons is involved in the regulation of neural development. The response of neuronal TLR7 to ssRNAs may also be critical for the effects of prenatal infection on neural development.

In addition to bacterial and viral ssRNAs, TLR7 also recognizes self-mRNA and miRNA (Diebold et al., 2006; Lehmann et al., 2012a). During development, many neurons undergo cell death. In addition, mRNA and miRNA can be secreted into the extracellular environment through exosomes (Bobrie et al., 2011; Record et al., 2011). It is possible that neurons engulf cell debris and/or exosomes in their environment and then activate TLR7 in the endosomal pathway to impair dendritic or axonal growth. Neurons may then redirect their axons or dendrites to grow in a region without danger signals. In addition, the intracellular ma-

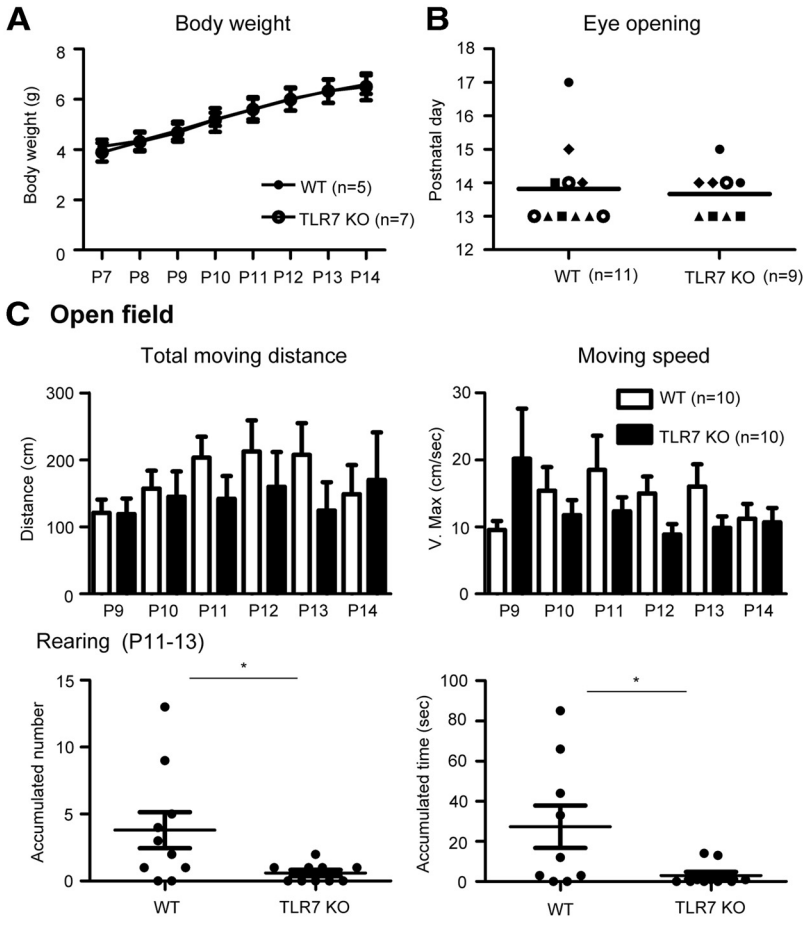

Figure 15. TLR7 knock-out mice exhibit lower exploratory activity. ***A***, Body weight of male TLR7 KO and WT mice from P7 to P14. Sample size (*n*) of each group is indicated. ***B***, Eye opening. The dates of eye opening of individual animals are shown. Littermates are indicated by the same shape spots. ***C***, Open field. The total moving distance and the moving speed were measured from P9 to P14. The total number of rears and time spent in on-wall rearing were recorded from P11 to P13. The data of individual animals are shown in ***B*** and the bottom of ***C***. The means + SEM are shown in ***A***, and in ***C***, bottom. The means ± SEM are shown in ***C***, top. $*p < 0.05$.

terials of distressed neurons may be recycled through autophagy, which then activates TLR7 in the endosomal pathway (Czirr and Wyss-Coray, 2012). TLR7 may impair axonal and dendritic extensions of distressed neurons and limit the interaction between distressed neurons and other neurons. Thus, ssRNA derived from either neighboring cells or intraneuronal distress can serve as a danger signal to remodel axonal and dendritic growth. A previous study estimated that peak cell death in the brain occurs before P10 (Gohlke et al., 2004). This also supports our hypothesis that TLR7 may recognize endogenous ligands during development and thus control neuronal morphogenesis before 3 weeks after birth. Our study also indicated that the growth of control neurons can catch up over time (from P14 to P21; Fig. 15*E*). This suggests that the effect of TLR7 knockdown *in vivo* promotes the maturation of neuronal development, but not the outgrowth after maturation.

Recently, evidence that has emerged supports the hypothesis that miRNAs secreted within exosomes act as paracrine signals to activate TLR7 in immune cells, which triggers a TLR-mediated prometastatic inflammatory response (Fabbri et al., 2012). In the nervous system, miRNAs are also shown to bind and activate TLR7, which may lead to neurodegeneration (Lehmann et al., 2012a,b). Therefore, it also seems possible that TLR7 expressed in the developing brain senses secreted miRNA and thus regulates neuronal development. More investigations need to be conducted to address this intriguing possibility.

The behavioral analyses conducted in this study further indicate that deletion of TLR7 influences the exploratory behavior of mice before 2 weeks after birth. It echoes the morphological difference at P7 and P14 in the *in vivo* knock-down experiment. It is certainly possible that developmental abnormality during the postnatal stage also has long-term impact on adult behaviors. It will thus be intriguing to investigate the behaviors of TLR7 KO mice at the adult stage. More learning/memory and cognitive analyses can then be performed to assess the physiological function of TLR7 in cognition. However, we need to emphasize here that global TLR7 KO mice were used in our study of behavioral assays. Thus, it is possible that glial and/or peripheral TLR7 also indirectly regulate cognition. To distinguish the contribution of neuronal, glial, and peripheral TLR7 to behavioral regulation, tissue- or cell-type-specific KO mice are required. More investigations have to be conducted to further address this point.

TLR7 versus TLR8

Although both TLR7 and TLR8 sense ssRNA and TLR8 is upregulated in TLR7 KO neurons, the compensation by TLR8 is incomplete. In cultured cortical neurons, the knockout of TLR7 still results in the promotion of dendrite and axon growth. It is possible that the level of TLR8 upregulation is not sufficient to completely compensate for the loss of TLR7. Another possibility is that TLR7 and TLR8 are not identical to each other in terms of their molecular functions in the regulation of neuronal morphogenesis. In dendritic cells, TLR7 is more effective at inducing the production of antiviral cytokines, while TLR8 tends to activate the expression of proinflammatory cytokines (Gorden et al., 2005). In contrast, our study suggests that TLR7 activation in neurons induced the expression of inflammatory cytokines, but not antiviral cytokines (Fig. 10). It will be interesting to further investigate the downstream cytokines produced by TLR8 activation in TLR7 KO neurons.

A previous study showed that intracerebroventricular injection of TLR7 agonists (CL075, loxoribine, and R837) induces expression of both inflammatory and antiviral cytokines, including IFN-β, in the brain (Butchi et al., 2008). However, in our cultured neurons, IFN-β was not noticeably induced by CL075 (Fig. 10). Perhaps, glial cells in the brain are the major cell population contributing to IFN-β expression. It echoes the possibility that different types of cells respond differentially to TLR7 agonists.

Specificity of various TLR7 agonists

R837, CL075, and loxoribine have been recognized as synthetic TLR7 agonists (Hemmi et al., 2002; Gorden et al., 2005, 2006a,b). R837 was applied in our preliminary screening that identified the

negative role of TLR7 in dendrite growth (Fig. 1). However, comparison of WT neurons with TLR7 KO neurons showed that R837 is not specific for TLR7 as it still impairs the dendritic arborization of TLR7 KO neurons (Fig. 8*A*). Additionally, other reports also identified nonspecific effects of R837. Administration of R837 results in the activation of transient receptor potential vanilloid 1 and the inhibition of background and voltage-gated potassium channels, which are independent of TLR7 (Kim et al., 2011; Lee et al., 2012). We therefore suggest that CL075 and loxoribine are better agonists for TLR7. In our study, CL075 is the more potent agonist of TLR7, with an effective concentration of just 4–6 μM—approximately 200-fold lower than that of loxoribine at 1 mM—and we therefore largely focused on its effects in our study.

The downstream signaling pathway of TLR7 in the regulation of neuronal morphology

Based on the downstream TIR domain containing adaptors, TLRs are categorized into two groups. One group is TRIF dependent, including TLR3 and TLR4; the other is Myd88 dependent, containing the rest of the TLRs. TLR4 also uses Myd88 to deliver the signal (Akira and Sato, 2003; Takeda and Akira, 2004; Kawai and Akira, 2006). Both TRIF and Myd88 deliver the signals to the downstream transforming growth factor-β-activated protein kinase 1 (TAK1). TAK1 then activates MAPK and IKK, and delivers the signals to transcription factors AP-1 and NF-κB. AP-1 and NF-κB then induce the expression of inflammatory cytokines (Kawai and Akira, 2006; Chevrier et al., 2011). Previous studies showed that Myd88 and NF-κB are not involved in the downregulation of neurite outgrowth via TLR8 and TLR3 (Ma et al., 2006; Cameron et al., 2007). However, in this study, we found that Myd88 is required for TLR7 downstream signaling to induce IL-6 expression and restrict dendrite growth. However, it is not clear what causes this conflict. As the examined TLRs were different, these TLRs might use different downstream molecules to regulate neuronal morphology. On the other hand, the previous studies focused on neurite outgrowth, a very early event in neuronal differentiation; here, we investigated the effect of TLR7 on dendrite arborization, which occurs later. It is also unclear whether TLRs use different adaptors in the regulation of different cellular events.

In addition to Myd88, our data also suggest that c-Fos and IL-6 act downstream of TLR7 in controlling dendrite growth. This suggests that in neurons TLR7 activation uses the canonical signaling pathway, namely the Myd88–c-Fos–IL-6 pathway, to inhibit dendrite outgrowth. Our data also suggest that IL-6 is required and sufficient for dendrite withdrawal mediated by TLR7 activation. Although TNF-α was also induced by TLR7 activation, deletion of TNF-α did not impair the effect of TLR7 activation, suggesting that TNF-α is not essential for TLR7-mediated downregulation of dendrite growth.

In conclusion, our study provides evidence that TLR7 negatively regulates dendrite and axon growth through the Myd88–c-Fos–IL-6 pathway. It also suggests that, like other cells, neurons also produce inflammatory cytokines by canonical innate immune pathways. In addition to their functions in innate immunity, these cytokines, especially IL-6, also regulate neuronal morphology. Therefore, neuronal innate immunity conducts multiple functions in brains.

References

Akira S, Sato S (2003) Toll-like receptors and their signaling mechanisms. Scand J Infect Dis 35:555–562. CrossRef Medline

Alexopoulou L, Holt AC, Medzhitov R, Flavell RA (2001) Recognition of double-stranded RNA and activation of NF-kappaB by Toll-like receptor 3. Nature 413:732–738. CrossRef Medline

Barrat FJ, Meeker T, Gregorio J, Chan JH, Uematsu S, Akira S, Chang B, Duramad O, Coffman RL (2005) Nucleic acids of mammalian origin can act as endogenous ligands for Toll-like receptors and may promote systemic lupus erythematosus. J Exp Med 202:1131–1139. CrossRef Medline

Bobrie A, Colombo M, Raposo G, Théry C (2011) Exosome secretion: molecular mechanisms and roles in immune responses. Traffic 12:1659–1668. CrossRef Medline

Bowie AG, Haga IR (2005) The role of Toll-like receptors in the host response to viruses. Mol Immunol 42:859–867. CrossRef Medline

Brown AS, Schaefer CA, Wyatt RJ, Goetz R, Begg MD, Gorman JM, Susser ES (2000) Maternal exposure to respiratory infections and adult schizophrenia spectrum disorders: a prospective birth cohort study. Schizophr Bull 26:287–295. CrossRef Medline

Butchi NB, Pourciau S, Du M, Morgan TW, Peterson KE (2008) Analysis of the neuroinflammatory response to TLR7 stimulation in the brain: comparison of multiple TLR7 and/or TLR8 agonists. J Immunol 180:7604–7612. Medline

Cameron JS, Alexopoulou L, Sloane JA, DiBernardo AB, Ma Y, Kosaras B, Flavell R, Strittmatter SM, Volpe J, Sidman R, Vartanian T (2007) Toll-like receptor 3 is a potent negative regulator of axonal growth in mammals. J Neurosci 27:13033–13041. CrossRef Medline

Chao TY, Raines RT (2011) Mechanism of ribonuclease A endocytosis: analogies to cell-penetrating peptides. Biochemistry 50:8374–8382. CrossRef Medline

Chen CY, Lin CW, Chang CY, Jiang ST, Hsueh YP (2011) Sarm1, a negative regulator of innate immunity, interacts with syndecan-2 and regulates neuronal morphology. J Cell Biol 193:769–784. CrossRef Medline

Chevrier N, Mertins P, Artyomov MN, Shalek AK, Iannacone M, Ciaccio MF, Gat-Viks I, Tonti E, DeGrace MM, Clauser KR, Garber M, Eisenhaure TM, Yosef N, Robinson J, Sutton A, Andersen MS, Root DE, von Andrian U, Jones RB, Park H, et al (2011) Systematic discovery of TLR signaling components delineates viral-sensing circuits. Cell 147:853–867. CrossRef Medline

Chung WC, Huang TN, Hsueh YP (2011) Targeted deletion of CASK-interacting nucleosome assembly protein causes higher locomotor and exploratory activities. Neurosignals 19:128–141. CrossRef Medline

Czirr E, Wyss-Coray T (2012) The immunology of neurodegeneration. J Clin Invest 122:1156–1163. CrossRef Medline

Diebold SS, Kaisho T, Hemmi H, Akira S, Reis e Sousa C (2004) Innate antiviral responses by means of TLR7-mediated recognition of single-stranded RNA. Science 303:1529–1531. CrossRef Medline

Diebold SS, Massacrier C, Akira S, Paturel C, Morel Y, Reis e Sousa C (2006) Nucleic acid agonists for Toll-like receptor 7 are defined by the presence of uridine ribonucleotides. Eur J Immunol 36:3256–3267. CrossRef Medline

Fabbri M, Paone A, Calore F, Galli R, Gaudio E, Santhanam R, Lovat F, Fadda P, Mao C, Nuovo GJ, Zanesi N, Crawford M, Ozer GH, Wernicke D, Alder H, Caligiuri MA, Nana-Sinkam P, Perrotti D, Croce CM (2012) MicroRNAs bind to Toll-like receptors to induce prometastatic inflammatory response. Proc Natl Acad Sci U S A 109:E2110–E2116. CrossRef Medline

Gauzzi MC, Del Cornò M, Gessani S (2010) Dissecting TLR3 signalling in dendritic cells. Immunobiology 215:713–723. CrossRef Medline

Gilmore JH, Fredrik Jarskog L, Vadlamudi S, Lauder JM (2004) Prenatal infection and risk for schizophrenia: IL-1beta, IL-6, and TNFalpha inhibit cortical neuron dendrite development. Neuropsychopharmacology 29:1221–1229. CrossRef Medline

Gohlke JM, Griffith WC, Faustman EM (2004) The role of cell death during neocortical neurogenesis and synaptogenesis: implications from a computational model for the rat and mouse. Brain Res Dev Brain Res 151:43–54. CrossRef Medline

Gorden KB, Gorski KS, Gibson SJ, Kedl RM, Kieper WC, Qiu X, Tomai MA, Alkan SS, Vasilakos JP (2005) Synthetic TLR agonists reveal functional differences between human TLR7 and TLR8. J Immunol 174:1259–1268. Medline

Gorden KK, Qiu XX, Binsfeld CC, Vasilakos JP, Alkan SS (2006a) Cutting edge: activation of murine TLR8 by a combination of imidazoquinoline

immune response modifiers and polyT oligodeoxynucleotides. J Immunol 177:6584–6587. Medline

Gorden KK, Qiu X, Battiste JJ, Wightman PP, Vasilakos JP, Alkan SS (2006b) Oligodeoxynucleotides differentially modulate activation of TLR7 and TLR8 by imidazoquinolines. J Immunol 177:8164–8170. Medline

Heil F, Hemmi H, Hochrein H, Ampenberger F, Kirschning C, Akira S, Lipford G, Wagner H, Bauer S (2004) Species-specific recognition of single-stranded RNA via toll-like receptor 7 and 8. Science 303:1526–1529. CrossRef Medline

Hemmi H, Takeuchi O, Kawai T, Kaisho T, Sato S, Sanjo H, Matsumoto M, Hoshino K, Wagner H, Takeda K, Akira S (2000) A Toll-like receptor recognizes bacterial DNA. Nature 408:740–745. CrossRef Medline

Hemmi H, Kaisho T, Takeuchi O, Sato S, Sanjo H, Hoshino K, Horiuchi T, Tomizawa H, Takeda K, Akira S (2002) Small anti-viral compounds activate immune cells via the TLR7 MyD88-dependent signaling pathway. Nat Immunol 3:196–200. CrossRef Medline

Hoebe K, Du X, Georgel P, Janssen E, Tabeta K, Kim SO, Goode J, Lin P, Mann N, Mudd S, Crozat K, Sovath S, Han J, Beutler B (2003) Identification of Lps2 as a key transducer of MyD88-independent TIR signalling. Nature 424:743–748. CrossRef Medline

Hornung V, Guenthner-Biller M, Bourquin C, Ablasser A, Schlee M, Uematsu S, Noronha A, Manoharan M, Akira S, de Fougerolles A, Endres S, Hartmann G (2005) Sequence-specific potent induction of IFN-alpha by short interfering RNA in plasmacytoid dendritic cells through TLR7. Nat Med 11:263–270. CrossRef Medline

Hou B, Reizis B, DeFranco AL (2008) Toll-like receptors activate innate and adaptive immunity by using dendritic cell-intrinsic and -extrinsic mechanisms. Immunity 29:272–282. CrossRef Medline

Huyton T, Rossjohn J, Wilce M (2007) Toll-like receptors: structural pieces of a curve-shaped puzzle. Immunol Cell Biol 85:406–410. CrossRef Medline

Iwasaki A (2007) Role of autophagy in innate viral recognition. Autophagy 3:354–356. Medline

Jenkins KA, Mansell A (2010) TIR-containing adaptors in Toll-like receptor signalling. Cytokine 49:237–244. CrossRef Medline

Kang JY, Lee JO (2011) Structural biology of the Toll-like receptor family. Annu Rev Biochem 80:917–941. CrossRef Medline

Kaul D, Habbel P, Derkow K, Krüger C, Franzoni E, Wulczyn FG, Bereswill S, Nitsch R, Schott E, Veh R, Naumann T, Lehnardt S (2012) Expression of Toll-like receptors in the developing brain. PLoS One 7:e37767. CrossRef Medline

Kawai T, Akira S (2006) TLR signaling. Cell Death Differ 13:816–825. CrossRef Medline

Kim SJ, Park GH, Kim D, Lee J, Min H, Wall E, Lee CJ, Simon MI, Lee SJ, Han SK (2011) Analysis of cellular and behavioral responses to imiquimod reveals a unique itch pathway in transient receptor potential vanilloid 1 (TRPV1)-expressing neurons. Proc Natl Acad Sci U S A 108:3371–3376. CrossRef Medline

Kopf M, Baumann H, Freer G, Freudenberg M, Lamers M, Kishimoto T, Zinkernagel R, Bluethmann H, Köhler G (1994) Impaired immune and acute-phase responses in interleukin-6-deficient mice. Nature 368:339–342. CrossRef Medline

Kumar H, Kawai T, Akira S (2009) Toll-like receptors and innate immunity. Biochem Biophys Res Commun 388:621–625. CrossRef Medline

Lathia JD, Okun E, Tang SC, Griffioen K, Cheng A, Mughal MR, Laryea G, Selvaraj PK, ffrench-Constant C, Magnus T, Arumugam TV, Mattson MP (2008) Toll-like receptor 3 is a negative regulator of embryonic neural progenitor cell proliferation. J Neurosci 28:13978–13984. CrossRef Medline

Lau CM, Broughton C, Tabor AS, Akira S, Flavell RA, Mamula MJ, Christensen SR, Shlomchik MJ, Viglianti GA, Rifkin IR, Marshak-Rothstein A (2005) RNA-associated autoantigens activate B cells by combined B cell antigen receptor/Toll-like receptor 7 engagement. J Exp Med 202:1171–1177. CrossRef Medline

Lee HK, Lund JM, Ramanathan B, Mizushima N, Iwasaki A (2007) Autophagy-dependent viral recognition by plasmacytoid dendritic cells. Science 315:1398–1401. CrossRef Medline

Lee J, Kim T, Hong J, Woo J, Min H, Hwang E, Lee SJ, Lee CJ (2012) Imiquimod enhances excitability of dorsal root ganglion neurons by inhibiting background (K(2P)) and voltage-gated (K(v)1.1 and K(v)1.2) potassium channels. Mol Pain 8:2. CrossRef Medline

Lehmann SM, Krüger C, Park B, Derkow K, Rosenberger K, Baumgart J, Trimbuch T, Eom G, Hinz M, Kaul D, Habbel P, Kälin R, Franzoni E, Rybak A, Nguyen D, Veh R, Ninnemann O, Peters O, Nitsch R, Heppner FL, et al (2012a) An unconventional role for miRNA: let-7 activates Toll-like receptor 7 and causes neurodegeneration. Nat Neurosci 15:827–835. CrossRef Medline

Lehmann SM, Rosenberger K, Krüger C, Habbel P, Derkow K, Kaul D, Rybak A, Brandt C, Schott E, Wulczyn FG, Lehnardt S (2012b) Extracellularly delivered single-stranded viral RNA causes neurodegeneration dependent on TLR7. J Immunol 189:1448–1458. CrossRef Medline

Lin YL, Lei YT, Hong CJ, Hsueh YP (2007) Syndecan-2 induces filopodia formation via the neurofibromin-PKA-Ena/VASP pathway. J Cell Biol 177:829–841. CrossRef Medline

Lund JM, Alexopoulou L, Sato A, Karow M, Adams NC, Gale NW, Iwasaki A, Flavell RA (2004) Recognition of single-stranded RNA viruses by Toll-like receptor 7. Proc Natl Acad Sci U S A 101:5598–5603. CrossRef Medline

Ma Y, Li J, Chiu I, Wang Y, Sloane JA, Lü J, Kosaras B, Sidman RL, Volpe JJ, Vartanian T (2006) Toll-like receptor 8 functions as a negative regulator of neurite outgrowth and inducer of neuronal apoptosis. J Cell Biol 175:209–215. CrossRef Medline

Maiorano NA, Mallamaci A (2009) Promotion of embryonic cortico-cerebral neuronogenesis by miR-124. Neural Dev 4:40. CrossRef Medline

Mariathasan S, Monack DM (2007) Inflammasome adaptors and sensors: intracellular regulators of infection and inflammation. Nat Rev Immunol 7:31–40. CrossRef Medline

Matsuda T, Cepko CL (2004) Electroporation and RNA interference in the rodent retina in vivo and in vitro. Proc Natl Acad Sci U S A 101:16–22. CrossRef Medline

Nishiya T, DeFranco AL (2004) Ligand-regulated chimeric receptor approach reveals distinctive subcellular localization and signaling properties of the Toll-like receptors. J Biol Chem 279:19008–19017. CrossRef Medline

O'Neill LA, Bowie AG (2007) The family of five: TIR-domain-containing adaptors in Toll-like receptor signalling. Nat Rev Immunol 7:353–364. CrossRef Medline

Pasparakis M, Alexopoulou L, Episkopou V, Kollias G (1996) Immune and inflammatory responses in TNF alpha-deficient mice: a critical requirement for TNF alpha in the formation of primary B cell follicles, follicular dendritic cell networks and germinal centers, and in the maturation of the humoral immune response. J Exp Med 184:1397–1411. CrossRef Medline

Patterson PH (2002) Maternal infection: window on neuroimmune interactions in fetal brain development and mental illness. Curr Opin Neurobiol 12:115–118. CrossRef Medline

Patterson PH (2009) Immune involvement in schizophrenia and autism: etiology, pathology and animal models. Behav Brain Res 204:313–321. CrossRef Medline

Record M, Subra C, Silvente-Poirot S, Poirot M (2011) Exosomes as intercellular signalosomes and pharmacological effectors. Biochem Pharmacol 81:1171–1182. CrossRef Medline

Rolls A, Shechter R, London A, Ziv Y, Ronen A, Levy R, Schwartz M (2007) Toll-like receptors modulate adult hippocampal neurogenesis. Nat Cell Biol 9:1081–1088. CrossRef Medline

Tabata H, Nakajima K (2008) Labeling embryonic mouse central nervous system cells by in utero electroporation. Dev Growth Differ 50:507–511. CrossRef Medline

Takeda K, Akira S (2004) TLR signaling pathways. Semin Immunol 16:3–9. CrossRef Medline

Whelan JA, Russell NB, Whelan MA (2003) A method for the absolute quantification of cDNA using real-time PCR. J Immunol Methods 278:261–269. CrossRef Medline

Zhao CT, Li K, Li JT, Zheng W, Liang XJ, Geng AQ, Li N, Yuan XB (2009) PKCdelta regulates cortical radial migration by stabilizing the Cdk5 activator p35. Proc Natl Acad Sci U S A 106:21353–21358. CrossRef Medline